NASA Contractor Report 174999

Thermomechanical Cyclic Hardening Behavior of Hastelloy-X

Paul A. Bartolotta
The University of Akron
Akron, Ohio

November 1985

Prepared for the
Lewis Research Center
Under Grant NAG 3-379

NASA
National Aeronautics and
Space Administration

TABLE OF CONTENTS

THERMOMECHANICAL CYCLIC HARDENING BEHAVIOR OF HASTELLOY-X

Paul A. Bartolotta
National Aeronautics and Space Administration
Lewis Research Center
Cleveland, Ohio 44135

SUMMARY

Experimental evidence of thermomechanical history dependence on the cyclic hardening behavior of a representative combustor liner material Hastelloy-X is presented, along with a discussion about the relevant concept of thermomechanical path dependence. Based on the experimental results, a discussion is given on the inadequacy of formulating "nonisothermal" constitutive equations solely on the basis of isothermal testing.

Finally, the essence of a mathematical representation of thermoviscoplasticity is presented that qualitatively accounts for the observed hereditary behavior. This is achieved by formulating the scaler evolutionary equation in an established viscoplastic theory to reflect thermomechanical path dependence. Although the necessary nonisothermal tests for further quantifying the thermoviscoplastic model have been identified, such data are not yet available.

1. INTRODUCTION

High-temperature energy system components (e.g., aircraft and rocket engine components, and nuclear reactor system components) not only experience mechanical loading but are also subjected to high thermal gradients and transients. These nonisothermal conditions are often severe enough to cause inelastic (thermomechanical) deformation which is the ultimate cause of structural failure in these components. Consider, as an example, an aircraft gas turbine engine combustor liner. Conventional combustor liners are constructed from sheet metal and experience extremely high thermal gradients and rapid thermal transients that induce large thermal stresses. These thermal stresses are often accompanied by significant inelastic deformation and, after repeated engine missions, can result in combustor liner distortion. If this distortion becomes large enough to cause the cooling air streams to be detoured from their engineered paths, the result can be over-heating and damage not only to the liner, but also to other critical components. The way to alleviate such problems is through improved design based on better predictions of material behavior. Unfortunately, most constitutive theories are unable to accurately predict inelastic material response under general thermomechanical conditions.

Almost all constitutive equations and damage models used in structural analysis and design for nonisothermal applications are based solely on data from isothermal tests. These isothermal tests are conducted over the temperature range of interest; material constants are then determined at each test temperature to furnish a "nonisothermal" representation. A question immediately comes to mind concerning the accuracy of this approach in describing nonisothermal (thermomechanical) behavior, i.e., one asks whether the formulation of a nonisothermal constitutive model can be based exclusively on isothermal experimentation. The answer to this question constitutes the main objective of this study. Toward this answer, a series of simple uniaxial tests have

been defined and conducted on the combustor liner material Hastelloy-X. A general description of these tests along with a discussion of the relevant concept of thermomechanical path dependence is presented in the next chapter. Chapter 3 presents a detailed description of the experimental procedure and the experimental results obtained in this study.

In Chapter 4, the essence of a mathematical representation of thermoviscoplasticity that attempts to qualitatively account for the observed thermomechanical behavior is presented. This is achieved by formulating the evolutionary equation for the scalar state variable in a known viscoplastic model (refs. 1 and 2) to reflect thermomechanical path dependence. Although candidate nonisothermal tests providing the necessary information to further quantify the thermoviscoplastic model have been identified, they will not be conducted until the presently expanding Structures Division Laboratory at NASA Lewis becomes operative. Finally, Chapter 5 presents a summary of the present study and conclusions drawn from it. Also, a brief discussion is given on suggested areas for further study.

2. THERMOMECHANICAL PATH DEPENDENCE - CONCEPT AND EXPERIMENTS

Cyclic hardening/softening is a feature of inelastic deformation that requires accurate representation in structural analysis and design. It is often characterized experimentally by conducting uniaxial tests at various fixed strain ranges ($\Delta\varepsilon$) and strain rates ($\dot{\varepsilon}$) (fig. 2.1). Hardening (or softening) is measured in terms of the stress range versus the number of cycles ($\Delta\sigma$ versus N).

In situations involving nonisothermal cycling an important question arises regarding the dependence of cyclic hardening on thermomechanical history. Figure 2.2 illustrates this concept in terms of a ($\Delta\sigma$,N,T) space, where T represents the temperature. As a thermomechanical path is followed from point 1 to point 2 in (N,T), the stress range changes by $\delta(\Delta\sigma)$. The question may be asked concerning whether $\delta(\Delta\sigma)$ depends on the thermomechanical path followed from point 1 to point 2. This question is equivalent to the question stated in the introductory chapter (i.e., can a nonisothermal deformation model be formulated solely on the basis of isothermal testing?) The answer to this question was identified earlier as a major objective of this study.

It is sometimes desirable to characterize thermomechanical hardening in somewhat more general terms as indicated in figure 2.3. There, a state variable K (e.g., the size of the yield surface) replaces the stress range $\Delta\sigma$, and a measure of accumulated inelastic deformation (or work) P replaces the cyclic count N. The latter replacement is made in an attempt to furnish a characterization of hardening that is valid for all strain ranges and rates. The key question remains unchanged in terms of figure 2.3 -- does the change in the variable δK depend on thermomechanical path?

A negative answer to this question implies that a unique surface K(P,T) exists in the (K,P,T) space of figure 2.3. Because then,

$$\delta K = \int_1^2 dK = \int_1^2 \frac{\partial K}{\partial P} dP + \frac{\partial K}{\partial T} dT \qquad (2.1)$$

and δK is independent of the path.

If a unique surface K(P,T) exists, evidently it can be defined by tests conducted along any thermomechanical path. In particular, the isothermal tests depicted in figure 2.4 will suffice. Thus, in this case, there is no need to conduct cyclic hardening tests any more complicated than isothermal ones; a complete characterization of cyclic thermoplastic hardening is possible on the basis of isothermal testing alone.

Conversely, a positive answer to the question posed above (i.e., δK does depend on the path), implies that no unique surface K(P,T) exists and, consequently, isothermal testing is not sufficient, in itself, to characterize nonisothermal cyclic hardening behavior.

A series of tests of the type depicted in figure 2.2 have been identified and conducted on the alloy Hastelloy-X with an aim of answering the questions raised in this and the previous chapter. The individual tests follow simple stepwise nonisothermal paths as illustrated in figure 2.5, including some paths that are isothermal. The following chapter gives a detailed description of the experimental procedure and test results.

3. EXPERIMENTATION

3.1 Introduction

In this chapter a complete description of the material Hastelloy-X is presented. Also, a description of the experimental apparatus and procedures is given. Finally, the test results are presented and discussed with emphasis on the nonisothermal data.

3.2 Test Plan

The plan was of a two-fold nature. First, initial data was obtained for Hastelloy-X from isothermal tests to create an isothermal data base of cyclic strain hardening tests at a temperature range of 427 to 760 °C (800 to 1400 °F). Secondly, attempting to answer the question posed in chapter 2 (i.e., can a complete nonisothermal representation be formulated based solely on isothermal test results?), a series of stepwise nonisothermal tests were conducted. Both isothermal and nonisothermal tests were conducted on Hastelloy-X over a longitudinal strain-range of $\pm$0.3 percent and a constant strain-rate of 10^{-3}/s. The temperatures used for isothermal tests were 427, 538, 593, 649, and 760 °C (800, 1000, 1100, 1200, and 1400 °F). The nonisothermal tests were conducted in a stepwise manner between two different test temperatures, 427 and 649 °C (800 and 1200 °F). By using these two test temperatures in different combinations with each other, several thermomechanical paths were followed. These thermomechanical paths, testing procedure, and temperature change techniques will be discussed later in this chapter.

3.3 Material

Experiments were conducted on a representative combustor liner material, Hastelloy-X. Hastelloy-X is an austenitic nickel-based superalloy used in components that require oxidation resistance up to 1204 °C (2200 °F). Specimens for the present study were fabricated from 19 mm (0.75 in.) diameter bar stock that originally came in 1.2 m (4 ft) sections supplied by the Aerojet Nuclear Systems Company (ANSC).

The chemical composition of the Hastelloy-X along with the appropriate AMS specifications are listed in table 3.1. The chemical composition values of the Hastelloy-X fell well within the specified values. The composition specification for sheet form and same for bar form of Hastelloy-X are given in AMS 5536G and AMS 5754F, respectively. Both specifications list the same specified values for chemical composition of Hastelloy-X.

The microstructure was observed, along with grain size measurements, by the use of photomicrographs (taken after heat treatment). These photomicrographs were obtained for both longitudinal and transverse sections at x100, x250, and x500 magnifications (figs. 3.1 to 3.3). Using the x100 magnification photomicrographs, the grain size was estimated by an intercept procedure in accordance with ASTM Designation E-112. From this intercept procedure it was found that the bar stock had a relatively fine grain size, in the range 4 to 5 ASTM units (table 3.2). A brief description of the intercept method used will be presented in section 1 of the appendix (A.1).

Hardness measurements were made by ANSC before heat treatment and by NASA Lewis after heat treatment (table 3.3). The hardness measurements taken by NASA Lewis were microhardness measurements that were converted to Rockwell B hardness numbers. The values of hardness for Hastelloy-X, both before and after heat treatment, are below the maximum value of 100 Rockwell B (241 Brinell) specified in AMS 5754F.

3.4 Specimen Details

Straight-section thermal-mechanical specimens were machined from the Hastelloy-X rod stock according to the dimensions given in figure 3.4. Once machined, these specimens were finish-ground in the test section of the specimen with finishing marks kept parallel to the longitudinal axis to eliminate circumferential scratches and marks. Caution was exercised to avoid overheating of the specimens during machining or grinding.

The specimens were then solution annealed in accordance to Aerospace Material Specifications (AMS) AMS-5754G. Details of this specification are as follows:

(1) Specimens were cleaned and degreased

(2) Specimens were then heated in two batches in an oven chamber with argon gas

(3) Batch number 1 reached a temperature of 1177 °C (2151 °F) for 30 min and batch number 2 reached a temperature of 1178 °C (2153 °F) for the same

amount of time. (Specification states: 1177±4 °C (2150±25 °F) for about 30 min.)

(4) Both batches were then "air cooled." (Specification states: cooling rate is to be air cooled or faster.)

After the solution annealing process was complete the specimens were micropolished. The test sections of each specimen were micropolished with finishing marks parallel to the longitudinal axis of the specimen. The surface finish of the test section of each specimen after polishing was a R.M.S. 4 finish.

3.5 Test Apparatus

The loading frame (fig. 3.5) used in the experiments was designed and built at NASA Lewis. It is rated for loads of ±9072 kg (±20 000 lb) and uses a die set to maintain rig alignment during specimen loading. An MTS 442 controller was used as the servocontroller for the rig. The specimen was attached to the loading frame with a split grip (fig. 3.6) which can accommodate button-head and threaded specimen ends. Cooling of the upper and lower grips was achieved by wrapping 9.5 mm (3/8 in.) copper tubing around the grips and running recirculating water through the tubing.

The calibration of the load cell and fine tuning of the load conditioner were accomplished by using a special calibration specimen and a SR-4 strain indicator. The calibration specimen has a square cross-section with strain gauges mounted on each of the four faces. Semiannually, both the calibration specimen and the SR-4 strain indicator are checked and adjusted for accuracy by the National Bureau of Standards (N.B.S.).

Longitudinal strains were measured by an MTS high temperature axial extensometer (fig. 3.7) with a 25.4 mm (1 in.) gauge length. For protection against the high test temperatures, the extensometer is water cooled and is equipped with a watercooled heat shield. Longitudinal displacements were sensed by pointed quartz probes. To assure that the probes did not slip, dimples were made on the specimen and the probe points were placed in these dimples.

Calibration of the extensometer was carried out on a biaxial calibration fixture (fig. 3.8). Longitudinal displacements can be measured up to 1.27×10^{-3} mm (50 millionths of an inch (0.000050 in.)) with the calibration fixture. The range card for the strain conditioner was set up so that, ±10 V = ±10 mil (0.010). The calibration was checked after every other test.

The tests were performed in strain control over a longitudinal strain range of ±0.3 percent at a constant strain rate of 10^{-3}/s. To control the tests in strain control, a Wavetek waveform generator (Model 175) was used. The wave shape programmed into the generator was a triangular wave with an electrical signal of ±3 V. The electrical signal is the command input signal that the servosystem is made to follow.

Elevated specimen temperatures were achieved by high frequency induction heating. The induction unit used was a Lepel 2.5 kW high frequency generator with a Research Institute Panel Packer (Model 61011) for a temperature

controller. High temperatures were sensed with the use of Chromel-Alumel thermocouples which were spot-welded to the specimen. One thermocouple was used as a feedback control for the Panel Packer and another one was used to monitor the temperature with the aid of a Doric Trendicator.

An extensive thermal gradient study was conducted to assure that the temperature distribution over the specimen gauge length was within ± 5 °C (± 10 °F) of the nominal test temperature. This study concentrated mainly on the coil design for the induction heating. It was decided that the only two design limitations of the coil would be: (1) the coils diameter was large enough to allow the specimen to slip through it; (2) the coil must have adequate openings between the "turns" of the coil that would allow the extensometer probes to have "unrestrictive movement". With the aid of a specially thermocoupled specimen (fig. 3.9), several coil configurations were tried. The design giving best results was a seven turned coil of 3.18 mm (1/8 in.) flattened copper tubing. The coil turns spacing was such that there were three turns above the upper probe of the extensometer, one turn in between the upper and lower probes, and three turns below the lower probe (fig. 3.6(b)). Figure 3.9 shows the final temperature gradient achieved by the subject coil. The temperature gradient was checked for all test temperatures, and was frequently verified during the testing program.

Measurements of load and strain were taken with the aid of a strip chart recorder and an X-Y recorder (fig. 3.10). The X-Y recorder was used for recording load versus strain (hysteresis loops). The strip chart recorder was used to obtain stress range and number of cycles for strain hardening curves. For further information on specimens, grips, loading frame, strain measurements, temperature measurements, and other laboratory conditions, see reference 3.

3.6 Test Procedure

The test procedure used in the experimentation was in accordance with ASTM Designation E606-80 for constant-amplitude low-cycle fatigue testing. Exceptions along with specific details of the cited standard will be discussed in this section. Emphasis will be placed on the method used for temperature changes.

As previously stated, the mode of control used for the testing was longitudinal strain at ± 0.3 percent with a constant strain rate of 10^{-3}/s. The control generator used a triangular wave of ± 3 V. Test temperatures were 427, 538, 593, 649, and 760 °C (800, 1000, 1100, 1200, and 1400 °F) which were controlled by using a thermocouple.

All tests were conducted in an air environment. To compensate for air currents that would fluctuate the specimen temperature, plexiglass shields were placed around the specimen. Test preparation consisted of first making sure that the initial condition of "zero-load zero-strain" existed for the specimen. Then the specimen was heated to the appropriate test temperature and maintained at these conditions until temperature saturation was reached and thermal expansion had stabilized (elapsed time 20 min). Care went into making sure that a target value of +0.3 percent strain was reached and recorded for the first tensile half-cycle. This was important because unlike fatigue testing, the initial cycles are needed for a good strain hardening analysis. Initial

preparation for both isothermal and nonisothermal testing was done exactly alike.

For the isothermal tests, cycling was continued until fatigue failure had occurred. This avoided premature termination of the test, thus giving confidence in the experimental "saturated" stress range value for the test temperature. Repeatability of the isothermal material behavior for each test temperature was confirmed by repeating the isothermal test and by using initial cyclic data of the nonisothermal tests.

For the nonisothermal tests, cycling was continued until a predetermined number of cycles had been reached. At this time the temperature was changed and cycling continued until fatigue failure occurred. All temperature changes were performed using the following procedure:

(1) With the use of the X-Y recorder, line "A" is drawn tangent to the hysteresis loop with a slope E; Modulus of Elasticity; (fig. 3.11).

(2) Line "B" is drawn parallel to line "A" and intersects the point of origin.

(3) As the X-Y recorder's pen intersects line "B" at point "C" the test is then stopped. On achieving a zero stress-strain state, the control mode is switched from strain to load.

(4) At this point the new temperature is dialed into the controller and the specimens test temperature is changed.

(5) After reaching thermal equilibrium, the control mode is switched back to strain and cycling resumed. This procedure insures that the specimen is not subjected to any effects (i.e., creep) that may influence the results for the strain hardening analysis.

3.7 Test Results

3.7.1 Isothermal results. - Figure 3.12 shows the results of isothermal cyclic hardening tests conducted over a strain range of ± 0.3 percent and at a constant strain rate of 10^{-3}/s. The results show that the stress range and hardening rates have maxima at intermediate temperatures in the range tested.

As seen in figures 3.12 and 3.13 the saturation strength peaks at about 593 °C (1100 °F). Figure 3.13 shows that at an intermediate number of cycles, e.g., 1500 cycles, and well before saturation, the strength peak occurs at about 649 °C (1200 °F). At temperatures above the hardening peak the cyclic strength decreases markedly.

Up to about 1500 to 2000 cycles (fig. 3.12), the hardening rate (i.e., the change in stress range with numbers of cycles) is greatest at 649 °C (1200 °F). This rate increases for temperatures from 427 to 649 °C (800 to 1200 °F) and decreases rapidly above 649 °C (1200 °F).

Although it is not entirely correct to construct curves connecting isothermal data points as indicated in figure 3.13, this is commonly done. Such curves imply that the change of strength with temperature for a fixed number

of cycles is positive at temperatures below the hardness peak and negative for temperatures above it. Contrary to this implication of the isothermal tests, the results of nonisothermal tests will show that the rate of change of strength with temperature at a fixed number of cycles is always negative.

It is believed that the trends identified in the isothermal data are influenced by the phenomenon of "dynamic strain aging." This is discussed in section 2 of the appendix (A.2). Similar behavior has been observed in other common solid solution hardening alloys such as Alloy 800 H, 304, and 316 stainless steel (refs. 4 to 8).

3.7.2 Nonisothermal results. - The results of a sequence of stepwise nonisothermal tests of the type depicted in figure 2.5 are presented in figures 3.14 to 3.21. Each of the tests consisted of isothermal segments in which the temperature was held constant at either 427 or 649 °C (800 or 1200 °F). In each figure the two isothermal curves corresponding to 427 and 649 °C are shown as solid curves; the nonisothermal paths are shown dotted. The end points of each solid or dotted curve represents failure of the specimen. No special emphasis should be placed on the failure characteristics of any of the test results, as prevention of premature failures was not a primary concern in this study. Unfortunately, premature failures were usually caused by either the thermocouples themselves or the bands used to support the thermocouples.

Figure 3.14 shows the results of a test where the specimen was first cycled at 649 °C for 800 cycles; the temperature was then changed to 427 °C and cycling continued to failure at approximately 3500 cycles. Note that an increase in stress range (path AB) occurs as a result of the temperature change from 649 to 427 °C. This is contrary to the implication of the isothermal data and obviously cannot be predicted by that data alone. The nonisothermal trajectory OABC clearly does not lie on a surface defined by the isothermal curves.

In the context of figure 2.5, the strengths $\Delta\sigma^{(a)}$ and $\Delta\sigma^{(b)}$ are not equal for the test of figure 3.14. Making this comparison at N = 2000 cycles (point C), $\Delta\sigma^{(a)}$ and $\Delta\sigma^{(b)}$ differ by almost 150 MPa. The difference in saturated stress ranges of the nonisothermal test OABC (terminating at 427 °C) and the 427 °C isothermal test is not as large but still in the order of 50 MPa; note that this comparison is made at vastly different numbers of cycles.

In figure 3.15 the initial temperature was 649 °C for the first 1600 cycles then the temperature was abruptly changed to 427 °C and cycling continued until the specimen failed. Again, note that as the temperature was decreased from 649 to 427 °C the stress range (path DE) increased by approximately 80 MPa. As before, path ODEF does not lie on a surface defined by the isothermal data. The saturated stress range values for the nonisothermal test ODEF and the 427 °C isothermal test differ by approximately 75 MPa.

The results of a two step thermomechanical path is presented in figure 3.16. Here, cycling starts at 427 °C to 800 cycles, changed to 649 °C for another 400 cycles, and then the temperature is changed back to 427 °C for the remainder of the test. Once again, contrary to the isothermal data, this figure shows that an increase in temperature results in a decrease in strength ($\Delta\sigma$) and vice versa.

The previous figures (figs. 3.14 to 3.16) presented results of thermomechanical paths that terminated at 427 °C. Figures 3.17 to 3.19 show results for paths terminating at 649 °C. In figure 3.17 initial cycling was conducted at 427 °C for 400 cycles then the temperature was increased to 649 °C for the rest of the test. As seen, the final saturated strength is approximately the same as that of the isothermal value for 649 °C. Nevertheless, an increase in temperature again results in a decrease in the stress range (path LM) and path OLMN does not lie on a surface defined by isothermal data.

From figure 3.17, the saturated stress range seems not to be influenced strongly by the nonisothermal path OLMN. Another similar test was performed (fig. 3.18), this time initial cycling at 427 °C was continued for 1600 cycles at which time the temperature was increased to 649 °C and cycling continued. Still, the nonisothermal path OPQR had no significant effect on the saturated strength. However, there is surely no possibility of predicting the hardening response up to saturation on the basis of isothermal information. A third test was performed with initial cycling at 427 °C continued up to near saturation (7000 cycles) before the temperature was changed to 649 °C (fig. 3.19). Again, the saturated strengths for the isothermal and nonisothermal tests are nearly identical and, again, the hardening behavior is not predictable from isothermal data.

The complete thermomechanical response to saturation displayed in figures 3.14 to 3.19 is very complicated. Adding to the complication is the premature failure of some of the specimens. Toward somewhat simplifying the picture, emphasis will now be placed on the early hardening behavior, up to 2000 cycles, where all of the specimens were still intact. This is justified in that the principal focus of this study is on thermoplastic deformation behavior, not failure. Clearly, the understanding and representation of the deformation response through the first 2000 cycles is pertinent to conducting accurate structural analyses.

Figure 3.20 is a collection of previously shown results in which the thermomechanical paths end up at 427 °C at 2000 cycles. Isothermal data for 427 and 649 °C are shown as solid curves in figure 3.20. Note that the points F, C, K and 2 in figure 3.20 all represent cyclic strengths (stress ranges) for 427 °C at 2000 cycles, each of which having been reached by a different thermomechanical path. The range of strengths at 427 °C is close to 170 MPa.

Results of thermomechanical paths ending at 649 °C at 2000 cycles are presented in figure 3.21. Again, the solid curve represents isothermal tests. Points N, R, and 1 correspond to 649 °C strengths at 2000 cycles following different thermomechanical paths. The range of strengths here is close to 50 MPa.

With the help of figures 3.20 and 3.21 the questions posed in chapters 1 and 2 can be answered. The current hardness (strength) does depend upon the particular temperature-strain (thermomechanical) path followed. In the context of chapter 2, no unique surface K(P,T) as illustrated in figure 2.4, appears to exist, and the change in hardness (δK) does depend on thermomechanical path. Therefore, <u>isothermal testing is not sufficient, in itself, to characterize nonisothermal cyclic hardening behavior</u>. This section will be closed by listing the important features of the results discussed above:

(1) An increase in temperature always results in a decrease in strength (stress range) and a decrease in temperature always results in an increase in strength. This is contrary to the implications from the isothermal data.

(2) The current cyclic strength depends on the temperature-strain history (thermomechanical history).

(3) The information contained in the isothermal data is not sufficient to represent the hardening behavior under nonisothermal conditions.

4. THERMOMECHANICAL REPRESENTATION

4.1 Introduction

The experimental results presented in chapter 3 demonstrate thermomechanical path dependence in the cyclic hardening behavior of Hastelloy-X. Similar behavior has been found in both 304 and 316 stainless steels (refs. 4 to 7). In this chapter, the basis of a possible representation of this hereditary behavior is proposed through modification of a known viscoplastic model. A brief discussion of classical and unified viscoplasticity is first given after which the subject viscoplastic model (refs. 1 and 2) is described. A general discussion is then given of the modifications and additions required to extend the stated model to correctly characterize thermoviscoplasticity.

For a full understanding of the theories discussed, some knowledge of the fundamentals of continuum mechanics, elasticity and plasticity is required. Therefore, an overview of these fundamentals is included in appendix (A.3).

4.2 Viscoplasticity

Classical plasticity theory is applicable to metals at relatively low temperatures, but for high temperature applications, there is a need for more comprehensive representations of deformation behavior. At elevated temperatures, time and rate are important. Viscoplasticity includes dependency on time and rate as part of the material description.

The classical approach to viscoplasticity is to additively combine time-independent plasticity and time-dependent creep. Thus, in the total strain rate there is a separate term for creep strain rate (appendix (A.3)):

$$\dot{\varepsilon}_{ij} = \dot{\varepsilon}^{e}_{ij} + \dot{\varepsilon}^{P}_{ij} + \dot{\varepsilon}^{C}_{ij} \tag{4.1}$$

where $\dot{\varepsilon}^{e}_{ij}$, $\dot{\varepsilon}^{P}_{ij}$, and $\dot{\varepsilon}^{C}_{ij}$ represent components of elastic, plastic, and creep strain rate, respectively.

Classically, the plastic strain rate $\dot{\varepsilon}^{P}_{ij}$ and the creep strain rate $\dot{\varepsilon}^{C}_{ij}$ have separate flow laws. The flow laws for $\dot{\varepsilon}^{P}_{ij}$ and $\dot{\varepsilon}^{C}_{ij}$ have the following forms:

$$\dot{\varepsilon}^{P}_{ij} = F_{ijkl}(\sigma_{rs}, h^{P}_{\alpha})\dot{\sigma}_{kl} \tag{4.2}$$

and

$$\dot{\varepsilon}^{C}_{ij} = G_{ij}(\sigma_{kl}, h^{C}_{\alpha}) \tag{4.3}$$

where h^{P}_{α} is a measure of the history of plastic deformations; h^{C}_{α} is a measure of the history of creep.

Although there have been many attempts to account for creep-plasticity interaction by allowing the respective classical flow laws (equations (4.2) and (4.3)) each to depend in a limited way on both h^{P}_{α} and h^{C}_{α}, this has often fallen far short of adequately representing the inherent time and rate dependency of both creep and plasticity. A more realistic approach is followed in the unified theory.

4.3 Unified Viscoplastic Model

The major distinction between the unified approach and classical theory is that the plastic strain rate $\dot{\varepsilon}^{P}_{ij}$ and the creep rate $\dot{\varepsilon}^{C}_{ij}$ are incorporated into just one rate called the inelastic strain rate $\dot{\varepsilon}^{I}_{ij}$. Therefore, the total strain rate takes the following form:

$$\dot{\varepsilon}_{ij} = \dot{\varepsilon}^{e}_{ij} + \dot{\varepsilon}^{I}_{ij} \tag{4.4}$$

where $\dot{\varepsilon}^{e}_{ij}$ is the elastic strain rate and $\dot{\varepsilon}^{I}_{ij}$ is the inelastic strain rate which is inherently time dependent.

A general form of a unified viscoplastic model can be represented as follows:

(1) The flow law,

$$\dot{\varepsilon}^{I}_{ij} = f_{ij}(\sigma_{kl} - \alpha_{kl}, K) \tag{4.5}$$

where $\dot{\varepsilon}^{I}_{ij}$ is the inelastic strain rate, σ_{kl} is the applied stress, α_{lk} is a tensorial state variable and K is a scalar state variable.

(2) The evolutionary laws for state variables α_{ij} and K are, of the form,

$$\dot{\alpha}_{ij} = h^{\alpha}\dot{\varepsilon}^{I}_{ij} - r^{\alpha}\alpha_{ij} \tag{4.6}$$

and

$$\dot{K} = h^K (\dot{\varepsilon}^I_{kl}) - r^K \tag{4.7}$$

where h^α, h^K, γ^α and γ^K are work hardening and recovery functions. These functions (h^α, h^K, γ^α and γ^K) depend on stress, temperature, and the inelastic state variables. In terms of the stress rate a unified model takes the form:

$$\dot{\sigma}_{ij} = C_{ijkl}(\dot{\varepsilon}_{kl} - \dot{\varepsilon}^I_{kl} - \beta_{kl}\dot{T}) \tag{4.8}$$

where C_{ijkl} are the components of elastic stiffness, β_{kl} is the coefficient of thermal expansion and $\dot{T}$ the temperature rate.

Using equations (4.5) to (4.8) with well chosen constants and mathematical functions in the flow and evolutionary laws, the high-temperature behavior of metals can be accurately predicted. Recently, there have been many unified models formulated. For the purpose of this study one such model will be presented in more detail. A discussion will then be made of its extension to thermoviscoplasticity.

4.4 Robinson Model

4.4.1 Unified viscoplastic model. - The flow law in the Robinson viscoplastic theory (refs. 1 and 2) is written (appendix (A.4)):

$$2\mu\dot{\varepsilon}_{ij} = f(F)\frac{\Sigma_{ij}}{\sqrt{J_2}} \tag{4.9}$$

where $\dot{\varepsilon}_{ij}$ denotes the components of inelastic strain-rate, μ is a material parameter, f and F are material functions and J_2 is the second principal invariant of the effective stress,

$$\Sigma_{ij} = s_{ij} - a_{ij} \tag{4.10}$$

as defined in the appendix (A.4).

For an initially isotropic material, the stress dependence enters through,

$$F = \frac{J_2}{k^2} - 1 \tag{4.11}$$

F plays the role of a Bingham-Prager yield function in which k denotes the Bingham threshold shear stress below which the inelastic strain rate vanishes. In this state variable description, k is a scalar state variable accounting for isotropic hardening effects and α_{ij} are the components of a tensorial state variable (internal stress) accounting for kinematic effects.

It is assumed here that the gradual hardening (or softening) that accumulates over several cycles under cyclic stressing occurs isotropically, and therefore can be described in terms of the single scalar state variable k. That is not to say that kinematic (induced anisotropic) effects are not strongly present during cycling as the internal dislocation structure alters with immobilization and remobilization of dislocations under repeated stress reversals.

Since the experimental testing in this study is uniaxial, equation (4.11) is written in uniaxial terms using,

$$J_2 = \frac{(\sigma - \alpha)^2}{3} \tag{4.12}$$

thus

$$F = \frac{(\sigma - \alpha)^2}{K} - 1 \tag{4.13}$$

where σ and α denote the uniaxial components of the applied and internal (back) stress, and $K = 3k^2$. The concern of this section is the specification of an appropriate form of evolutionary law for K in equation (4.13) that reflects the thermomechanically hereditary behavior observed in figures 3.12 to 3.21 and in 304 and 316 stainless steel as cited in references 4 to 7.

In the subsequent development, isotropic hardening, through K, is dependent on inelastic work,

$$P = \int s_{ij} d\varepsilon_{ij} \tag{4.14}$$

however, the formulation is not innately limited to dependence on P and could, if appropriate, be taken to depend on some other scalar measure of mechanical deformation, say

$$\varphi = \int \sqrt{d\varepsilon_{ij} d\varepsilon_{ij}} \tag{4.15}$$

In figure 4.1, a schematic representation of a typical cyclic hardening response under some fixed strain range and strain rate is shown. This is qualitatively in keeping with the material response observed in figures 3.12 to 3.21 and with the physical arguments made in appendix (A.2). Figure 4.1 can be interpreted as a plot of $\Delta\sigma$ versus N (stress range versus number of cycles) or, in terms of chapter 2, K versus P for isothermal cycling (solid curves) at the three temperatures $T_1 < T_2 < T_3$. Figure 4.2, which is a plot of $\Delta\sigma$ or K versus temperature T, shows the commonly observed "strain-aging peak."

Classically, K has been taken as an explicit function of P and T, (e.g., ref. 9). As discussed in chapter 2, this implies the existence of a unique surface $K(P,T)$ (figure 2.4) that can be determined fully on the basis of isothermal hardening curves. This is equivalent to adopting the evolutionary equation for K as

$$dK = \frac{\partial K}{\partial P} dP + \frac{\partial K}{\partial T} dT \tag{4.16}$$

which is a perfect differential and integrable independently of the thermomechanical path $P(T)$ as described by equation (2.1). A candidate representation of the isothermal curves of figures 4.1 and 4.2 and the surface $K(P,T)$ in figure 2.4 is:

$$K(P,T) = K_s(T) + [K_i(T) - K_s(T)]e^{-P/P_o(T)} \tag{4.17}$$

The functions $K(0,T) = K_i(T)$ and $K(\infty,T) = K_s(T)$ are as illustrated in figure 4.2. The function $P_o(T)$ determines the temperature dependent cyclic hardening rate.

4.4.2 Thermoviscoplastic representation. - The classical representation described in the previous section clearly does not reflect the thermomechanical path dependence apparent in the test data of figures 3.12 to 3.21. Actual data show that the strength does significantly depend on thermal-strain history. Furthermore, the classical description permits an increase in strength with an increase in temperature in the neighborhood of the "strain-aging peak" (fig. 4.2). Nonisothermal data shows that an increase in temperature is always accompanied by a decrease in strength, i.e., a decrease in K.

A general form of evolutionary equation for K in equation (4.13) that can allow for thermomechanical history dependence of the cyclic hardening response is the following:

$$dK = \Gamma(P,T)dP + \Theta(P,T)dT \tag{4.18}$$

Equation (4.18) represents a kinetic growth law for K which is not a perfect differential and is integrable only when the thermomechanical path $P(T)$ is known. The functions $\Gamma(P,T)$ and $\Theta(P,T)$ are independent and not related as $\partial K/\partial P$ and $\partial K/\partial T$ are in equation (4.16). The function $\Gamma(P,T)$ can be determined on the basis of isothermal testing whereas $\Theta(P,T)$ cannot. A complete description of the nonisothermal hardening behavior in terms of equation (4.18) necessarily involves nonisothermal testing.

Candidate nonisothermal tests providing definitive information about the function $\Theta(P,T,)$ are beyond the scope of this study. However, tests of this nature have been identified in references 4 and 5.

A critical feature of the evolutionary law expressed in equation (4.18) is that it permits the cyclic hardening, in particular the current strength, to be dependent on thermomechanical history. This feature is evident in studies on 304 and 316 stainless steels and also according to this study on Hastelloy-X. Further details of this representation are discussed in reference 9.

5. SUMMARY

5.1 Summary and Conclusions

A question concerning the adequacy of formulating nonisothermal deformation models based exclusively on isothermal data was posed in chapter 1 and re-examined in chapter 2. In chapter 2, a general description of the experimental tests required to answer this question was given, along with a theoretical discussion about thermomechanical path dependence.

Descriptions of the experimental apparatus and procedures along with an extensive material characterization study was presented in chapter 3. Experimental results showing the dependence of thermomechanical history in cyclic hardening behavior of Hastelloy-X were also examined. Such cyclic behavior is believed to be influenced by metallurgical changes, i.e., dynamic strain aging (ref. 10 and appendix (A.2)). On this basis a discussion was given of the inadequacy of formulating "nonisothermal" constitutive relationships solely on the basis of isothermal test data, which is often done in practice.

The discussion in section 4.2 concerned the modeling of high temperature cyclic behavior using classical plasticity and classical viscoplasticity. Also, the concept of a unified viscoplastic representation was discussed.

A thermoviscoplastic model by Robinson was presented that attempts to qualitatively account for the observed hereditary cyclic hardening behavior. This was accomplished by appropriately reformulating the evolutionary equation for the scalar state variable in an established viscoplastic theory to reflect thermomechanical path dependence. Although the necessary nonisothermal tests for further quantifying the thermoviscoplastic model have been tentatively identified, such data are not yet available.

For the material Hastelloy-X the following conclusions can be drawn based on the present study:

(1) Concerning the question posed in chapter 1, it can be said that the information contained in isothermal cyclic hardening data is not sufficient to predict hardening behavior under general thermomechanical (nonisothermal) conditions.

(2) It is evident that the current strength under cyclic conditions depends upon thermomechanical history. This is also true for other materials, such as 304 and 316 stainless steel (refs. 1 to 4).

(3) The thermoviscoplastic representation presented here qualitatively accounts for the thermomechanical path dependence observed in the simple nonisothermal tests that were performed in this study.

5.2 Recommendations for Further Study

The results from this study show that the representation of nonisothermal cyclic hardening/softening behavior cannot be based exclusively on isothermal data. This was shown through the use of some simple nonisothermal tests. On this basis, the author wishes to acknowledge that this study has only

scratched the surface of this problem. There are many areas of study and future research that are needed in order to predict such behavior accurately. The following is a list of suggested areas to start off with:

(1) As it was resolved that the formulation of nonisothermal deformation models cannot be based exclusively on isothermal data, the question then arises - What nonisothermal tests are needed to supply the proper information for a complete nonisothermal representation? As stated previously, tentative nonisothermal tests have been identified but will not be conducted until the presently expanding Structures Division Laboratory at NASA Lewis becomes operative.

(2) In the spirit of this study, the following areas should be explored: (a) different stepwise thermomechanical paths using the same general conditions but other temperatures, (b) other strain rates and strain ranges, and (c) various heat treatments of the material.

(3) In this study only very simple forms of nonisothermal tests were considered (one- and two-step temperature changes). The next evolutionary step should be an attempt to simulate more realistic thermal cycles using a computer controlled system.

APPENDIX

A.1 Intercept Method for Estimating Grain Size

An intercept method created by J.E. Hilliard (ref. 11) is presented here. This procedure produces an estimate of the ASTM grain size of a microstructure with quite good accuracy. In this intercept method, the number of grain boundaries intersected by a superimposed outline (a line or a circle) are counted. Then by the use of the following equation, the ASTM grain size number is calculated:

$$G.S. = -10.00 + 6.64 \log\left(\frac{NM}{L}\right) \qquad (1)$$

where N is the number of intersections, M is the magnification of the micrographs, and L is the total length of the superimposed figure in centimeters.

Using a superimposed line gives a good approximation of the grain size but to minimize the standard deviation of the method and ultimately improving the accuracy a circle should be used as the superimposed figure. Whichever figure (line or circle) is used, the size of that figure should be related to the magnification of the micrograph such that the average number of intersections per application exceeds six. And to really obtain a good grain size approximation the total number of intersections should be more than 35.

A.2 Thermomechanical History Dependence and Metallurgical Change

It is well known that cyclic hardening of some structural alloys within their temperature range of interest is influenced by the phenomenon of dynamic strain aging (ref. 10). Strain aging occurs in solid solutions where solute atoms (e.g., carbon, nitrogen, etc.) are particularly free to diffuse through the parent lattice. It is energetically preferable for these solute atoms to occupy sites in the neighborhood of mobile dislocations where their presence immobilizes the dislocations or at least makes their movement difficult, thus causing strengthening.

Isothermal cycling at temperatures where such metallurgical changes occur might therefore be expected to show abnormal hardening, i.e., higher hardening rates and greater saturation strengths than at temperatures both lower and higher. Macroscopic evidence of strain aging in the alloy Hastelloy-X is shown in figure 3.12. Similar behavior in stainless steels has been reported in references 4 to 7.

From figure 3.12 the hardening rate and the stress range at "saturation" are maximal at an intermediate temperature in the range. This hardening peak is interpreted as a manifestation of dynamic strain aging. At lower temperatures the mobility of solute atoms is far less and strain aging cannot occur; at higher temperatures normal recovery processes, e.g., climb of edge dislocations, take over.

In the aging process described dislocations can break away from their "Cottrell solute atmospheres" becoming mobile again. Although temporarily freed, dislocations can again be immobilized as solute atoms gradually diffuse

back to them. As the thermally activated process of diffusion is involved and solute atoms are migrating to dislocations which themselves are moving under the applied stress, it is not surprising that the ensuing inelastic deformation (cyclic hardening in particular) has a complex dependence on thermomechanical history.

A.3 Basic Theory

A.3.1 Introduction. - In recent years, considerable research has been conducted in the development of unified viscoplastic models (or theories) for representing the inelastic deformation behavior of metals. To understand these models, one must have a basic knowledge of the fundamentals of continuum mechanics, elasticity, and plasticity. The purpose of this section of the appendix is to describe briefly the fundamental ideas and basic theories behind viscoplasticity.

A.3.2 Concepts of stress and (small) strain tensors. - Considering an arbitrary point in a continuum, the state of stress (stress state) and the state of strain (strain state) can be represented in tensor notation as: the stress tensor:

$$\sigma_{ij} = \begin{bmatrix} \sigma_{xx} & \sigma_{xy} & \sigma_{xz} \\ \sigma_{yx} & \sigma_{yy} & \sigma_{yz} \\ \sigma_{zx} & \sigma_{zy} & \sigma_{zz} \end{bmatrix} \tag{1}$$

and the strain tensor:

$$\varepsilon_{ij} = \begin{bmatrix} \varepsilon_{xx} & \varepsilon_{xy} & \varepsilon_{xz} \\ \varepsilon_{yx} & \varepsilon_{yy} & \varepsilon_{yz} \\ \varepsilon_{zx} & \varepsilon_{zy} & \varepsilon_{zz} \end{bmatrix} \tag{2}$$

where $i = 1,2,3$ or x,y,z and $j = 1,2,3$ or x,y,z. Both σ_{ij} and ε_{ij} are symmetrical tensors and only six components are required to describe the state of stress and corresponding strain at a point.

Experiments indicate that yielding and plastic deformation of metals are essentially independent of the applied "hydrostatic stress" ($\sigma_{xx}/3 + \sigma_{yy}/3 + \sigma_{zz}/3 = \sigma_{ii}/3$). Therefore, it is helpful to decompose the stress tensor into two parts, a hydrostatic part and a deviatoric part. The stress dependence is then taken in terms of the deviatoric stress tensor which is defined as:

$$s_{ij} = \sigma_{ij} - \frac{1}{3}\delta_{ij}\sigma_{kk} \tag{3}$$

Similarly, the deviatoric strain tensor is defined as:

$$e_{ij} = \varepsilon_{ij} - \frac{1}{3}\delta_{ij}\varepsilon_{kk} \tag{4}$$

where δ_{ij} is known as the Kronecker delta such that if $i = j$, $\delta_{ij} = 1$ and $i \neq j$, $\delta_{ij} = 0$. For an isotropic material the stress dependence can be taken in terms of invariants, i.e., quantities that are independent of the coordinate system. A set of scalar quantities called principal stress invariants are defined as:

$$I_1 = \sigma_{ii} \tag{5}$$

$$I_2 = \frac{1}{2} (\sigma_{ii}\sigma_{jj} - \sigma_{ij}\sigma_{ij}) \tag{6}$$

$$I_3 = \det |\sigma_{ij}| \tag{7}$$

I_1, I_2, and I_3 are called the first, second and third principal stress invariants, respectively. Likewise deviatoric stress invariants are defined as:

$$J_1 = S_{ii} = 0 \tag{8}$$

$$J_2 = \frac{1}{2} S_{ij}S_{ji} \tag{9}$$

$$J_3 = \frac{1}{3} S_{ij}S_{jk}S_{ki} \tag{10}$$

where J_1, J_2 and J_3 are the first, second and third deviatoric stress invariants.

A.3.3 Constitutive equations. - A.3.3.1 Overview: There are three conditions that the solution of a continuum mechanics problem must satisfy at each instant of time: These are:

(1) Equations of equilibrium; that relate body forces and surface tractions to stresses.

(2) Compatibility equations (geometry); these relate displacements to strains.

(3) Constitutive equations; which are relationships between stress, strain, time, temperature, etc.

The purpose of this section is to introduce the basic concepts of the third ingredient, constitutive equations, and to give a general overview of elasticity, and plasticity.

A.3.3.2 Elasticity: Subjecting a material to applied loads (stresses) will induce deformations. If the loads are removed and the material retains its original shape and size, then the material is called elastic. A general form of a constitutive model for a linear elastic material is "Generalized Hooke's Law" given by

$$\sigma_{ij} = C_{ijkl}\varepsilon_{kl} + B_{ij} \tag{11}$$

where C_{ijkl} is tensor of elastic constants; B_{ij} is initial stress tensor corresponding to a strain free state ($\varepsilon_{kl} = 0$). Assuming that the initial strain free state is also a stress free state then equation (11) becomes

$$\sigma_{ij} = C_{ijkl}\varepsilon_{kl} \tag{12}$$

The fourth order tensor C_{ijkl} consists of 81 constants. However, as σ_{ij} and ε_{ij} are both symmetric, it can be shown that there are 36 independent components in C_{ijkl}. Further conditions can be considered (i.e., thermodynamics, and material symmetry) and thus reduce the number of constants from 36 to 21, 13, 9, all the way down to 2 for an isotropic material.

For a linear elastic isotropic material equation (12) takes the form of:

$$\sigma_{ij} = \frac{E}{1 + \upsilon}\varepsilon_{ij} + \frac{\upsilon E}{(1 + \upsilon)(1 - 2\upsilon)}\varepsilon_{kk}\delta_{ij} \tag{13}$$

where υ is Poisson's ratio, E is Young's modulus. Similarly, for strain "Generalized Hooke's Law" can be given as:

$$\varepsilon_{ij} = D_{ijkl}\sigma_{kl} \tag{14}$$

where D_{ijkl} is a tensor of elastic constants which is the inverse of the material matrix C_{ijkl}. Likewise, for a linear elastic isotropic material equation (14) becomes:

$$\varepsilon_{ij} = \frac{1 + \upsilon}{E}\sigma_{ij} - \frac{\upsilon}{E}\sigma_{kk}\delta_{ij} \tag{15}$$

A.3.3.3 Plasticity: A material that is subjected to an applied loading (stress) will deform. If upon unloading the material's original shape and size are permanently distorted, it is said that the material has yielded plasticly. For example, in a uniaxial tensile test, the yield stress is defined as the point of stress below which the material's behavior is elastic (fig. A.1). In a multiaxial representation, a hypersurface is used to denote the limit of elastic behavior for a material, instead of a yield point (fig. A.2). When the material yields, or in other words, when the stress is such that the state of stress is out of the elastic region in figures A.1 and A.2, then the history of the stress path must be accounted for in the description of the yield surface. This is done with respect to increments of plastic strain. These concepts are the basic ideas behind the theory of plasticity.

A simplistic description of plastic strain can be comprehended by utilizing figure A.3. Total strain, which is shown graphically in figure A.3, can be mathematically represented as:

$$\varepsilon_{ij} = \varepsilon^{e}_{ij} + \varepsilon^{P}_{ij} \tag{16}$$

where ε^{e}_{ij} and ε^{P}_{ij} represents elastic and plastic strains respectively. Furthermore, it can be shown that the total strain increment can be given as:

$$d\varepsilon_{ij} = d\varepsilon^{e}_{ij} + d\varepsilon^{P}_{ij} \tag{17}$$

The yield surface of figure A.2 is mathematically represented by a yield function, a general form of this yield function can be given as:

$$F(\sigma_{ij}, H_{\alpha}) = 0 \tag{18}$$

where σ_{ij} is the stress state and H_{α} are state variables which measure of the history of plastic deformation. A stress state where $F = 0$ implies a plastic state, and a stress state where $F < 0$ implies an elastic state; $F > 0$ has no meaning.

Considering a strain hardening material, plastic strains are usually accompanied by a change in the yield surface in stress space. Accounting for such changes, the yield function (eq. (18)) must be formulated to correctly describe subsequent yield surfaces. As plastic deformation occurs $F = 0$ and therefore $dF = 0$. By differentiating equation (18) by the chain rule of calculus,

$$dF = \frac{\partial F}{\partial \sigma_{ij}} d\sigma_{ij} + \frac{\partial F}{\partial H\alpha} dH_{\alpha} = 0 \tag{19}$$

which is known as the consistency condition.

From the consistency condition criteria for loading, unloading, and neutral loading can be expressed. The loading criterion is given by

$$\frac{\partial F}{\partial \sigma_{ij}} d\sigma_{ij} > 0 \quad \text{and} \quad F = 0 \tag{20}$$

implying plastic strains occur and the yield surface changes. Neutral loading occurs when

$$\frac{\partial F}{\partial \sigma_{ij}} d\sigma_{ij} = 0 \quad \text{and} \quad F = 0 \tag{21}$$

implying no plastic strain and no change in the yield surface. The case where

$$\frac{\partial F}{\partial \sigma_{ij}} d\sigma_{ij} < 0 \quad \text{and} \quad F = 0 \tag{22}$$

is termed unloading, here the yield surface also remains unchanged.

In figure A.4, $\partial F/\partial \sigma_{ij}$ represents the outward normal to the yield surface $F = 0$ at a given stress state σ_{ij}. The inner product of $(\partial F/\partial \sigma_{ij})d\sigma_{ij}$ represents the magnitude of the component of $d\sigma_{ij}$ in the direction $\partial F/\partial \sigma_{ij}$.

As stated previously, a plastic strain in a material element results in a change in the yield surface, in other words, the material "hardens" or "softens." Because plastic strains are very load history dependent, plastic stress-strain relations are correctly expressed in terms of plastic strain

increments (incremental theories). The plastic strain increment $d\varepsilon_{ij}^{P}$ is linearly related to $\partial F/\partial\sigma_{ij}$ by,

$$d\varepsilon_{ij}^{P} = \lambda \frac{\partial F}{\partial \sigma_{ij}} \tag{23}$$

which is known as the normality condition. The normality condition states that the direction of $d\varepsilon_{ij}^{P}$ is in the direction of the outward normal of the yield surface $F = 0$. An expression that is used to describe the plastic strain increments is known as the "flow law." One more function is needed to complete the description of the consistency condition (eq. (19)) and that is known as the evolutionary law.

The evolutionary law is an expression that describes the growth in the state variable H_α as a function of the plastic strain increments. In its most general form, the evolutionary law is as follows.

$$dH_\alpha = f_{ij\alpha} d\varepsilon_{ij}^{P} \tag{24}$$

where $f_{ij\alpha}$ is a function of σ_{ij} and H_α.

To summarize, the basic concepts of the theory of plasticity are:

(1) A yield function (fig. A.4)

$$F(\sigma_{ij}, H_\alpha) = 0 \tag{25}$$

(2) The consistency equation,

$$dF = \frac{\partial F}{\partial \sigma_{ij}} d\sigma_{ij} + \frac{\partial F}{\partial H_\alpha} dH_\alpha = 0 \tag{26}$$

(3) An evolutionary law for H_α that has the form

$$dH_\alpha = f_{ij\alpha} d\varepsilon_{ij}^{P} \tag{27}$$

Using the evolutionary law (eq. (27)) and the normality condition, equation (26) assumes the form

$$dF = \frac{\partial F}{\partial \sigma_{ij}} d\sigma_{ij} + \frac{\partial F}{\partial H_\alpha} f_{ij\alpha} \lambda \frac{\partial F}{\partial \sigma_{ij}} = 0 \tag{28}$$

Solving for λ in equation (28) and substituting into the normality condition (eq. (23)),

$$d\varepsilon_{ij}^{P} = G \frac{\partial F}{\partial \sigma_{ij}} \frac{\partial F}{\partial \sigma_{kl}} d\sigma_{kl} \tag{29}$$

where

$$G = -\left(f_{rs\alpha} \frac{\partial F}{\partial \sigma_{rs}} \frac{\partial F}{\partial H_\alpha} \right)^{-1}$$

Equations (27) and (29) are the evolutionary law and the flow law, respectively. From these concepts two cases are considered:

Case I

$$\left.\begin{array}{l} \text{if } F = 0 \text{ and } \dfrac{\partial F}{\partial \sigma_{ij}} d\sigma_{ij} > 0 \\ \text{(loading)} \end{array}\right\} \text{then} \left\{\begin{array}{l} d\varepsilon^P_{ij} = G \dfrac{\partial F}{\partial \sigma_{ij}} \dfrac{\partial F}{\partial \sigma_{kl}} d\sigma_{kl} \\ dH_\alpha = f_{ij\alpha} d\varepsilon^P_{ij} \end{array}\right.$$

and the yield surface changes from $F(\sigma_{ij}, H_\alpha) = 0$ to $F(\sigma_{ij}, H'_\alpha) = 0$ with $H'_\alpha = H_\alpha + dH_\alpha$ (fig. A.4).

Case II

$$\left.\begin{array}{l} \text{if } F = 0 \text{ and } \dfrac{\partial F}{\partial \sigma_{ij}} d\sigma_{ij} \leq 0 \\ \text{(unloading and neutral loading)} \end{array}\right\} \text{then} \left\{\begin{array}{l} d\varepsilon^P_{ij} = 0 \\ dH_\alpha = 0 \end{array}\right.$$

therefore, no change in yield surface.

A.4 Robinson Model

Here Robinson's viscoplastic constitutive equations of references 6 and 7 is stated in nonisothermal and multiaxial form. These equations are valid for "small" deformations and initially isotropic materials.

$$2\mu\dot{\varepsilon}_{ij} = \begin{cases} \dfrac{F^n \Sigma_{ij}}{\sqrt{J_2}} ; & F > 0 \quad \text{and} \quad S_{ij}\Sigma_{ij} > 0 \\ 0 ; & F < 0 \quad \text{or} \\ & F > 0 \quad \text{and} \quad S_{ij}\Sigma_{ij} < 0 \end{cases} \tag{1}$$

$$\dot{a}_{ij} = \begin{cases} \dfrac{H}{G^\beta} \dot{\varepsilon}_{ij} - RG^{m-\beta} \dfrac{a_{ij}}{\sqrt{I_2}} ; & G > G_o \quad \text{and} \quad S_{ij}a_{ij} > 0 \\ \dfrac{H}{G_o^\beta} \dot{\varepsilon}_{ij} - RG_o^{m-\beta} \dfrac{a_{ij}}{\sqrt{I_2}} ; & G < G_o \quad \text{or} \quad S_{ij}a_{ij} < 0 \end{cases} \tag{2}$$

in which,

$$\Sigma_{ij} = S_{ij} - a_{ij} \tag{3}$$

$$S_{ij} = \sigma_{ij} - \frac{1}{3}\sigma_{kk}\delta_{ij} \tag{4}$$

$$a_{ij} = \alpha_{ij} - \frac{1}{3}\alpha_{kk}\delta_{ij} \tag{5}$$

$$F = \frac{J_2}{k^2} - 1 \tag{6}$$

$$G = \frac{I_2}{k_o^2} \tag{7}$$

$$J_2 = \frac{1}{2}\Sigma_{ij}\Sigma_{ij} \tag{8}$$

$$I_2 = \frac{1}{2}a_{ij}a_{ij} \tag{9}$$

Here, $\dot{\varepsilon}_{ij}$ denotes the components of inelastic strain rate, k and α_{ij} state variables and μ, n, m, β, R and H are material parameters, and k_o is the value of k at the reference temperature T_o.

The general form of the evolutionary law for the scalar state variable k (or $K = 3k^2$) is made in the foregoing text. This is further specified in reference 9 where it is assumed that all of the temperature dependence in the flow law (eq. (1)) resides in the state variable k. The recovery parameter R is taken as being strongly temperature dependent as also specified in reference 9.

REFERENCES

1. Robinson, D.N., "A Unified Creep-Plasticity Model for Structural Metals at High Temperature," ORNL/TM-5959, November 1978.

2. Robinson, D.N., and Swindeman, R.W., "Unified Creep-Plasticity Constitutive Equations for Structural Alloys at Elevated Temperature," ORNL/TM-8444, October 1982.

3. Hirschberg, M., "A Low Cycle Fatigue Testing Facility," Manual on Low Cycle Fatigue Testing, ASTM STP 465, American Society for Testing and Materials, 1969, p. 67.

4. Robinson, D.N., and Swindeman, R.W., "Additions and Modifications to Constitutive Equations in NE Standard F9-5Y," High-Temperature Structural Design Program Prog. Rep., ORNL-5794, June 1981.

5. Robinson, D.N., and Swindeman, R.W., "Modifications to Constitutive Equations in NE Standard F9-5T," High-Temperature Structural Design Program Prog. Rep., ORNL-5863, Dec. 1981.

6. Robinson, D.N., "Thermomechanical Deformation in the Presence of Metallurgical Changes," Proc. Second Symposium on Nonlinear Constitutive Relations for High Temperature Applications, NASA Lewis Research Center, Cleveland, Ohio, NASA Conf. Pub. 2271, June 1984.

7. Robinson, D.N., and Ellis, J.R., "High-Temperature Constitutive Modeling," Proc. Conf. on Turbine Engine Hot Section Technology, NASA Lewis Research Center, Cleveland, Ohio, NASA Conf. Pub. 2239, Oct. 1984.

8. Villagrana, R.E., Kaae, J.L., and Ellis, J.R., "The Effect of Aging and Cold Working on the High-Temperature Low-Cycle Fatigue Behavior of Alloy 800 H: Part II: Continuous Cyclic Loading," Metall. Trans. A, 1981, vol. 12A, p. 1849.

9. Robinson, D.N., and Bartolotta, P.A., "Viscoplastic Constitutive Relationships with Dependence on Thermomechanical History," NASA CR-174836, 1985.

10. Baird, J.D., "Dynamic Strain Aging," The Inhomogeneity of Plastic Deformation, ASM, Metals Park, Ohio, 1973.

11. Hilliard, J.E., "Estimating Grain Size by the Intercept Method," Metal Progress, May 1964, p. 99.

12. Drucker, D.C., "On Uniqueness in the Theory of Plasticity," Quarterly of Applied Mathematics, Vol. 14, 1956, pp. 35-42.

13. Drucker, D.C., "A Definition of Stable Inelastic Material," Journal of Applied Mechanics, Vol. 26, 1959.

14. Cailletaud, G., and Chaboche, J.L., "Macroscopic Description of the Microstructural Changes Induced by Varying Temperature: Example of IN 100 Cyclic Behavior," ICM, 33, Vol. 2, 1979.

15. Reid, S.R., and Ellis, J.R., "Multiaxial Exploratory Testing," High-Temperature Structural Design Program Prog. Rep., ORNL/5737, Dec. 1980.

16. Frederick, D., and Chang, T.S., Continuum Mechanics, Scientific Publishers, Inc., Cambridge, 1972.

17. Jaske, C., Rice, R., Buchheit, R., Roach, D., and Porfilio, T., "Low-Cycle Fatigue of Type 347 Stainless Steel and Hastelloy Alloy X in Hydrogen Gas and In Air at Elevated Temperatures," Battelle Laboratory Report NASA CR-135022, (NAS3-20078), Columbus, Ohio, 1976.

TABLE 3.1 - CHEMICAL COMPOSITION[a]

Element	ANSC[b]	AMS 5754F
C	0.08	0.05-0.15
Mn	.76	≤1.00
P	.001	≤0.040
S	.006	≤0.030
Si	.38	≤1.00
Cr	22.00	20.50-23.00
Ni	Remainder	Remainder
Mo	9.05	8.00-10.00
Cu	.01	----------
Fe	18.65	17.00-20.00
W	.43	0.20-1.00
Co	1.97	0.50-2.50
B	.001	≤0.010
Other		
Al	.01	----------
Ti	---------	----------
Zr	---------	----------
V	---------	----------

[a]Composition by percent weight (wt %).
[b]Values reported by Aerojet Nuclear Systems Company (ANSC).

TABLE 3.2 - ESTIMATED GRAIN SIZE AFTER HEAT TREATMENT[a]

Intercept method	ASTM grain size number	
	Longitudinal	Transverse
Average linear intercept	4.7	4.5
Circumference intercept	4.5	4.6

[a]In accordance with ASTM Designation: E-112.

TABLE 3.3 - HARDNESS VALUES

	Hardness numbers[a]	
	Before heat treatment[b]	After heat treatment
Longitudinal	87	--
Transverse	--	87
	--	89

[a]All table values indicated are Rockwell B hardness numbers.
[b]Measured by ANSC.

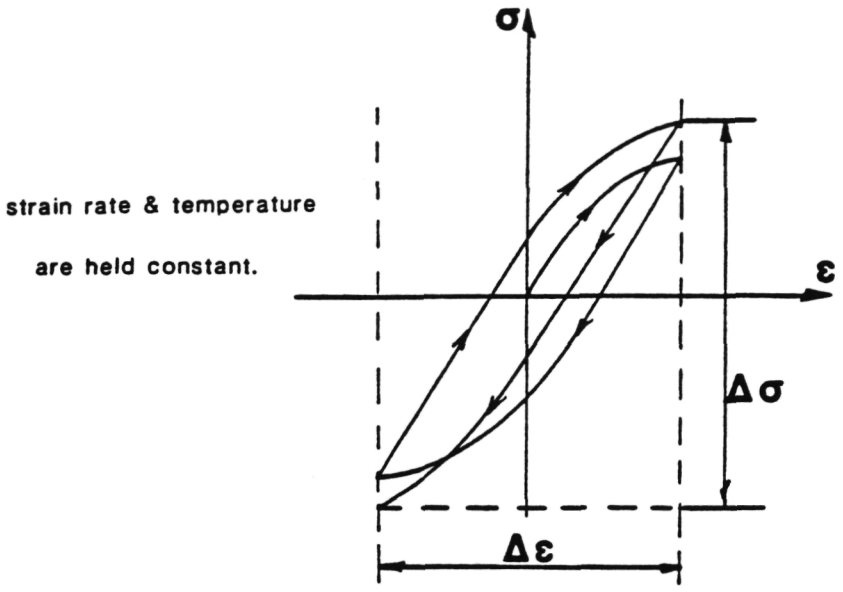

FIGURE 2.1 Hysteresis Loop

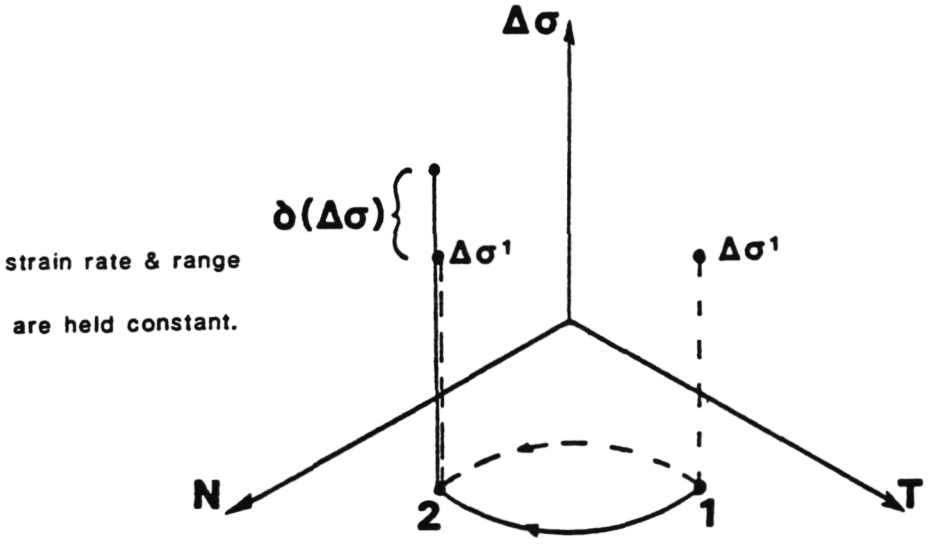

FIGURE 2.2 Does $\delta(\Delta\sigma)$ depend upon path?

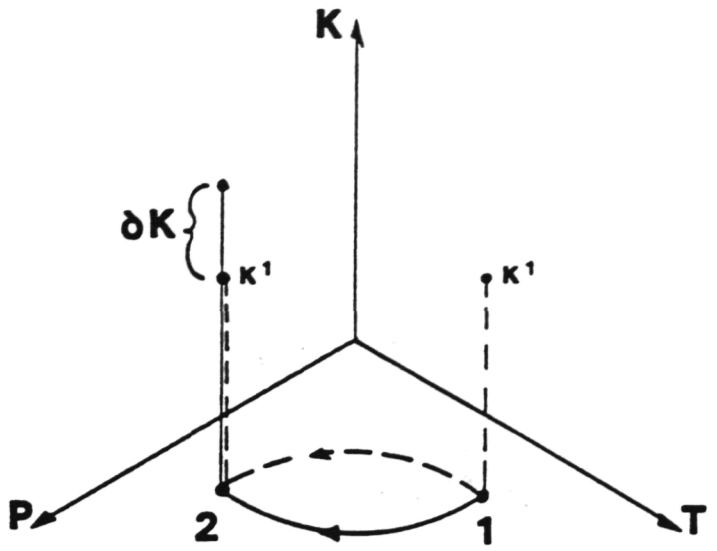

FIGURE 2.3 Does δK depend upon path?

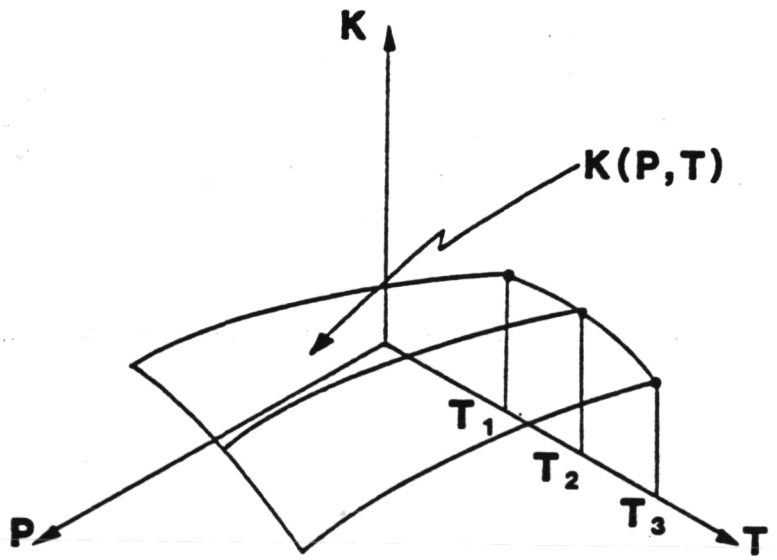

FIGURE 2.4 Surface K(P,T)

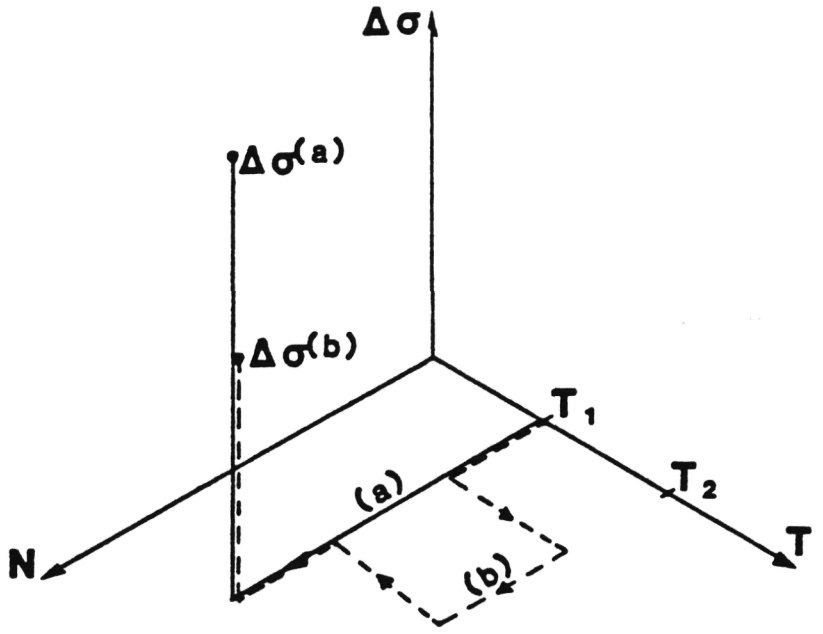

FIGURE 2.5 Stepwise Nonisothermal Path

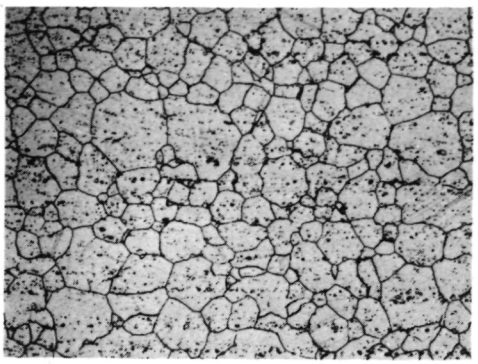

LONGITUDINAL

1 cm

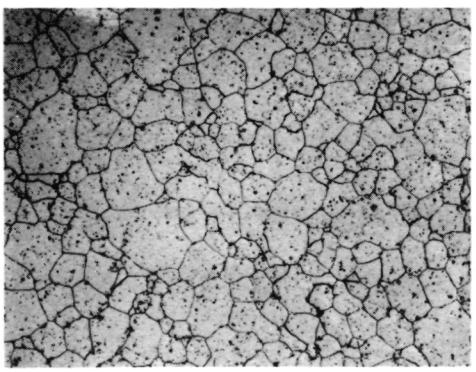

TRANSVERSE

Figure 3.1 HASTELLOY-X 100X Magnification

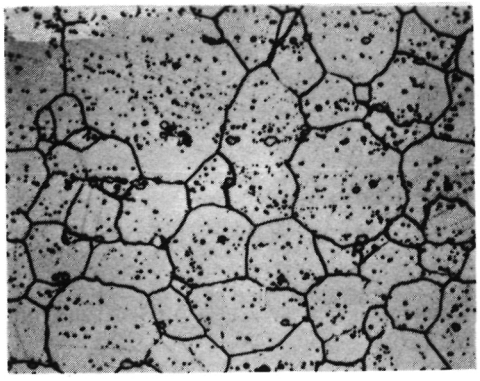

1 cm

LONGITUDINAL

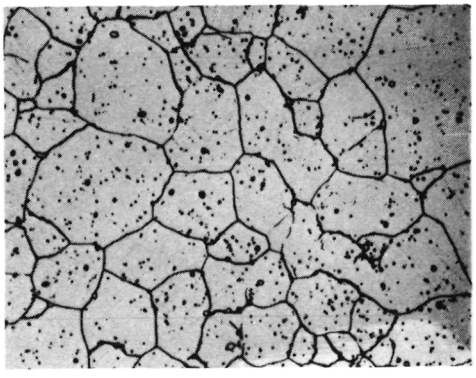

TRANSVERSE

Figure 3.2 HASTELLOY-X 250X Magnification

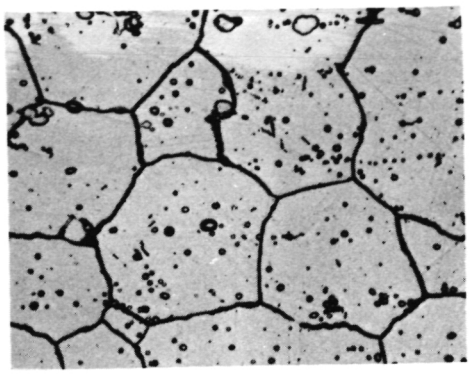

1 cm

LONGITUDINAL

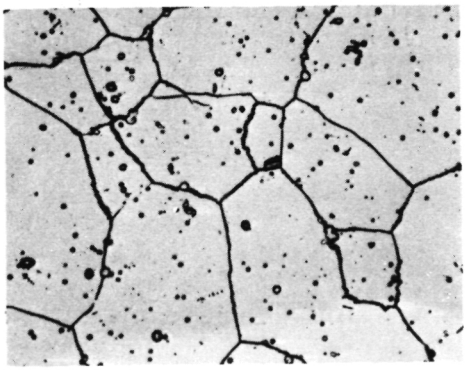

TRANSVERSE

Figure 3.3 HASTELLOY-X 500X Magnification

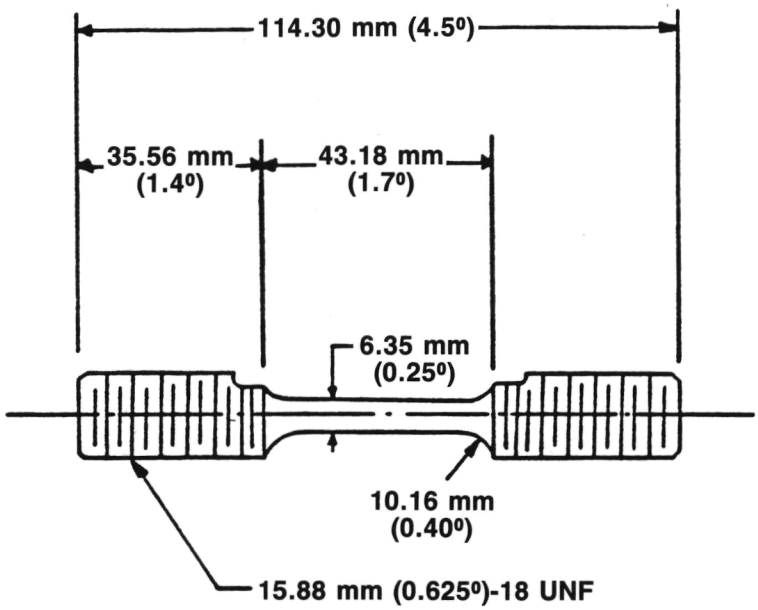

FIGURE 3.4 Uniaxial Specimen Dimensions.

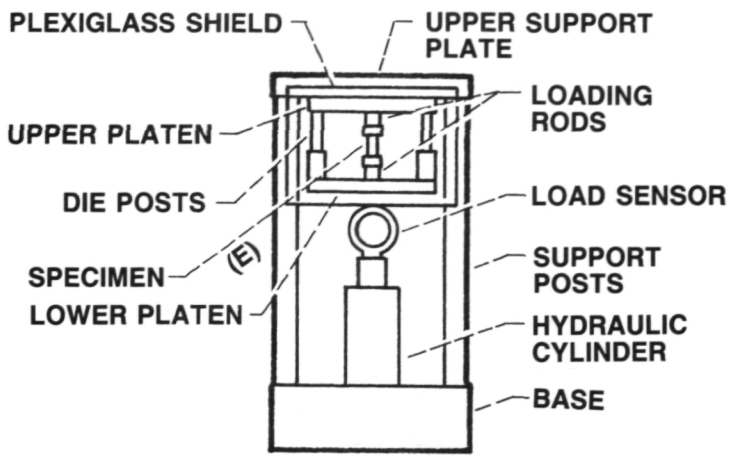

FIGURE 3.5a Load Frame Schematic.

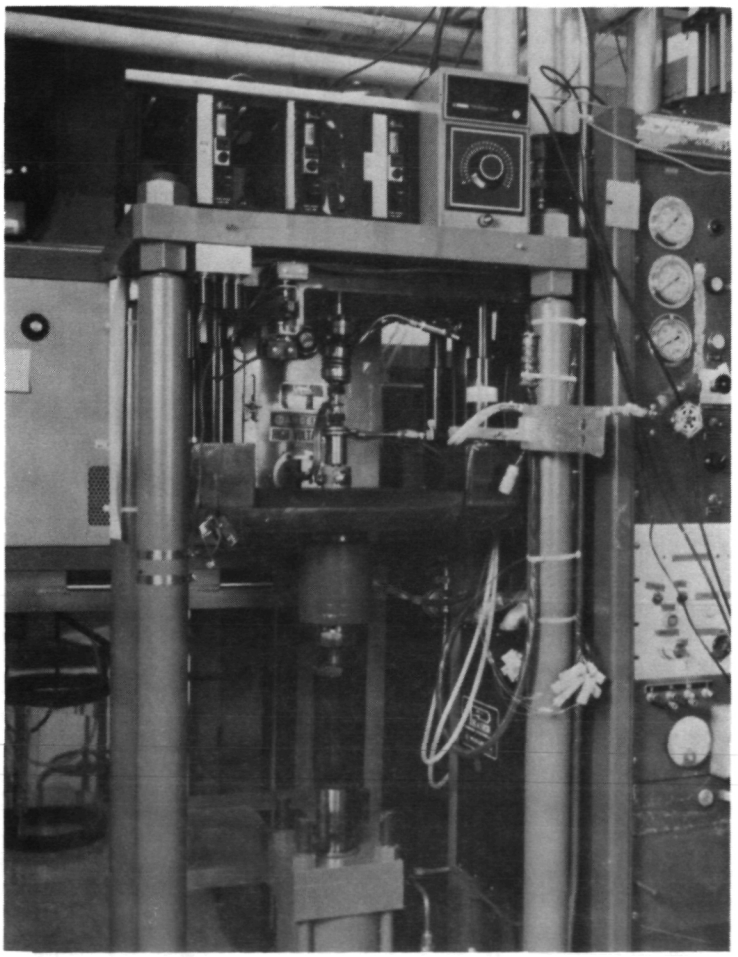

FIGURE 3.5b Actual Load Frame Set-up

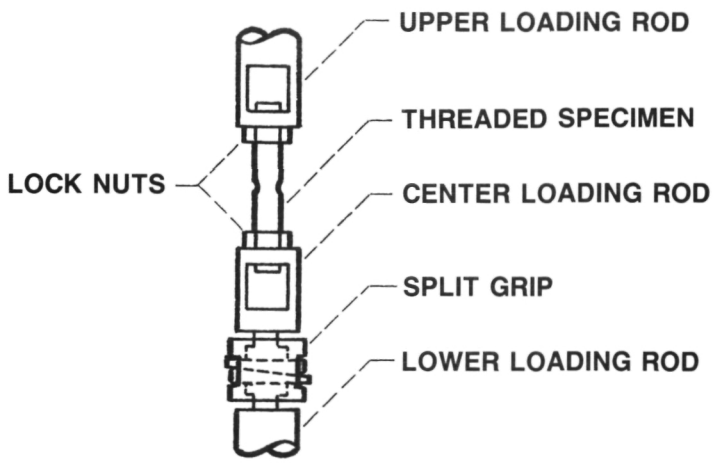

FIGURE 3.6a Assembly for Threaded Specimen.

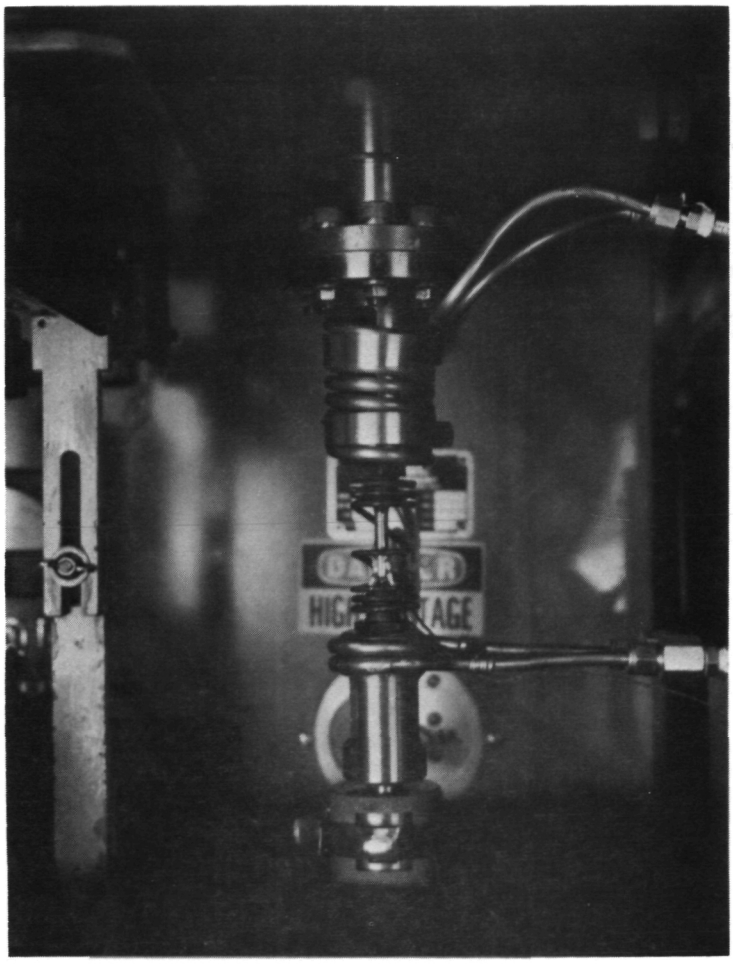

FIGURE 3.6b Actual Specimen Assembly

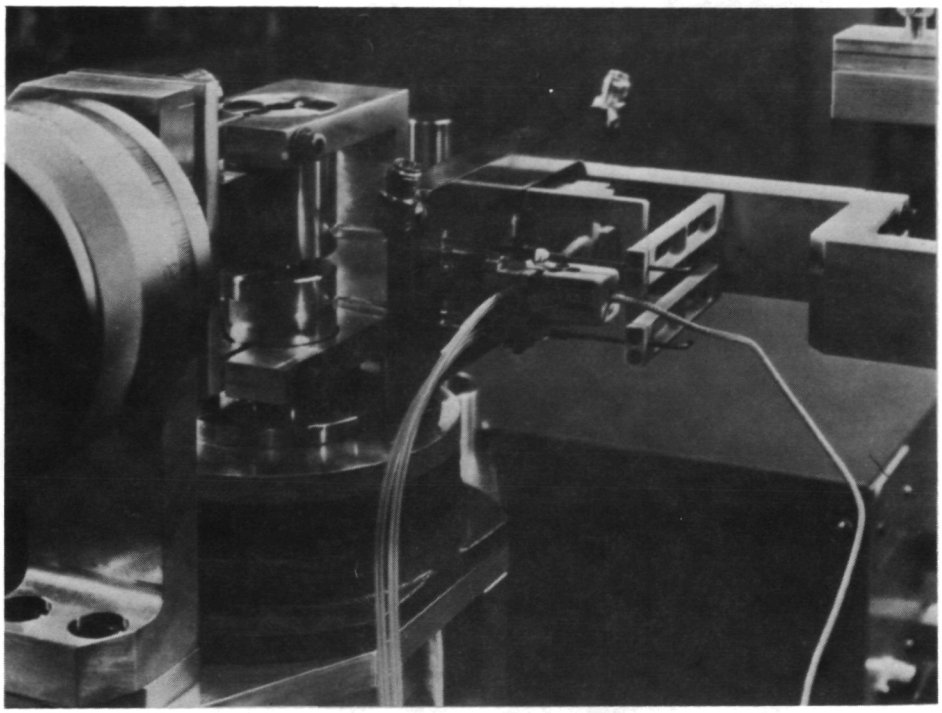

FIGURE 3.7 MTS Axial Extensometer

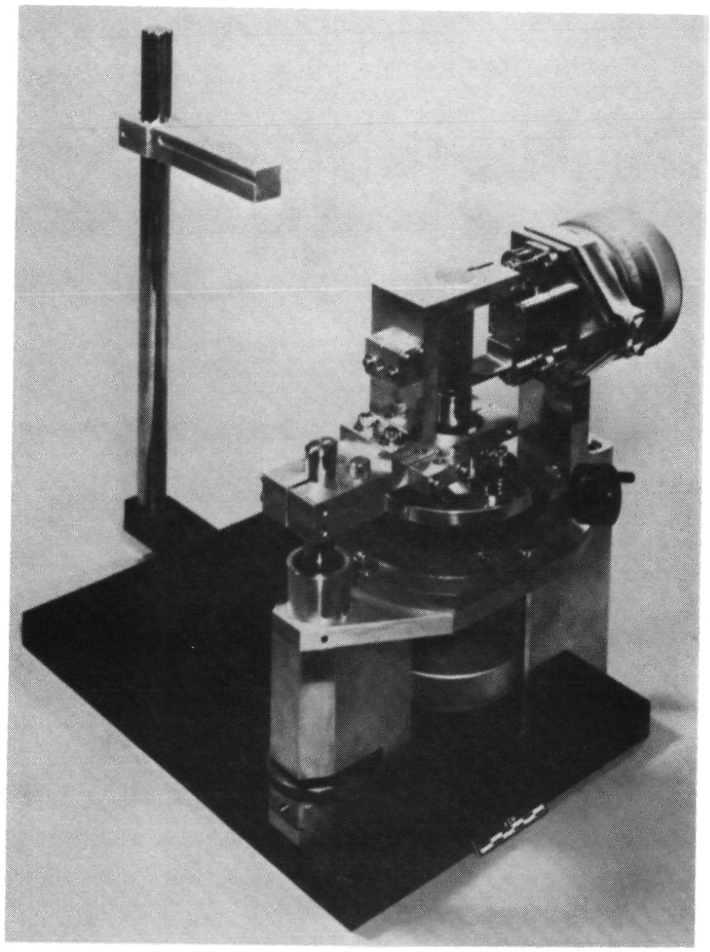

FIGURE 3.8 Biaxial Calibration Fixture

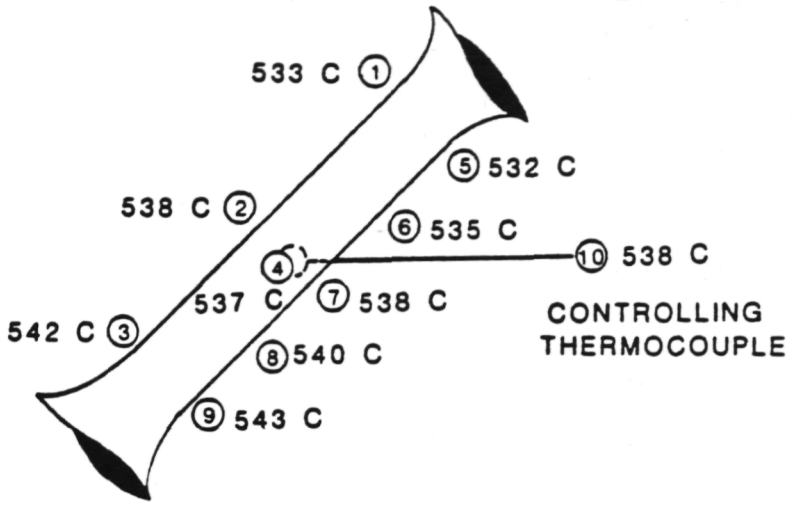

FIGURE 3.9 Thermal Gradient Profile

FIGURE 3.10 Control Room Set-up

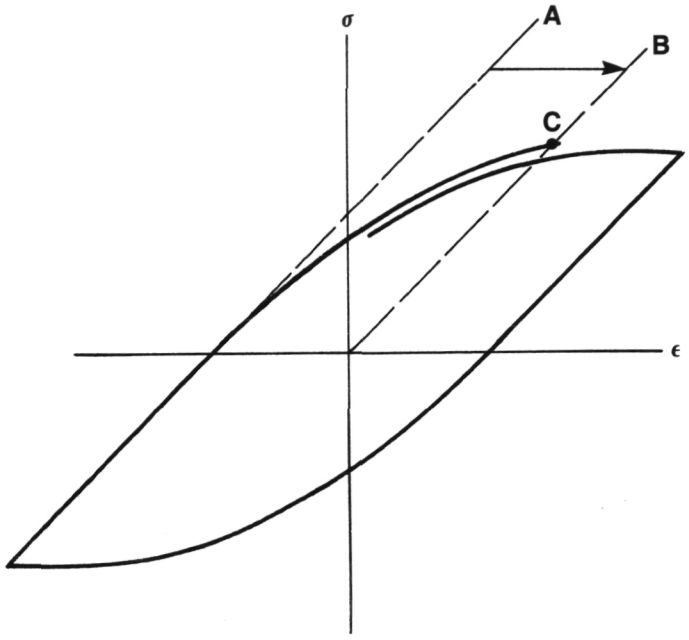

FIGURE 3.11 Zero-load Zero-strain Procedure

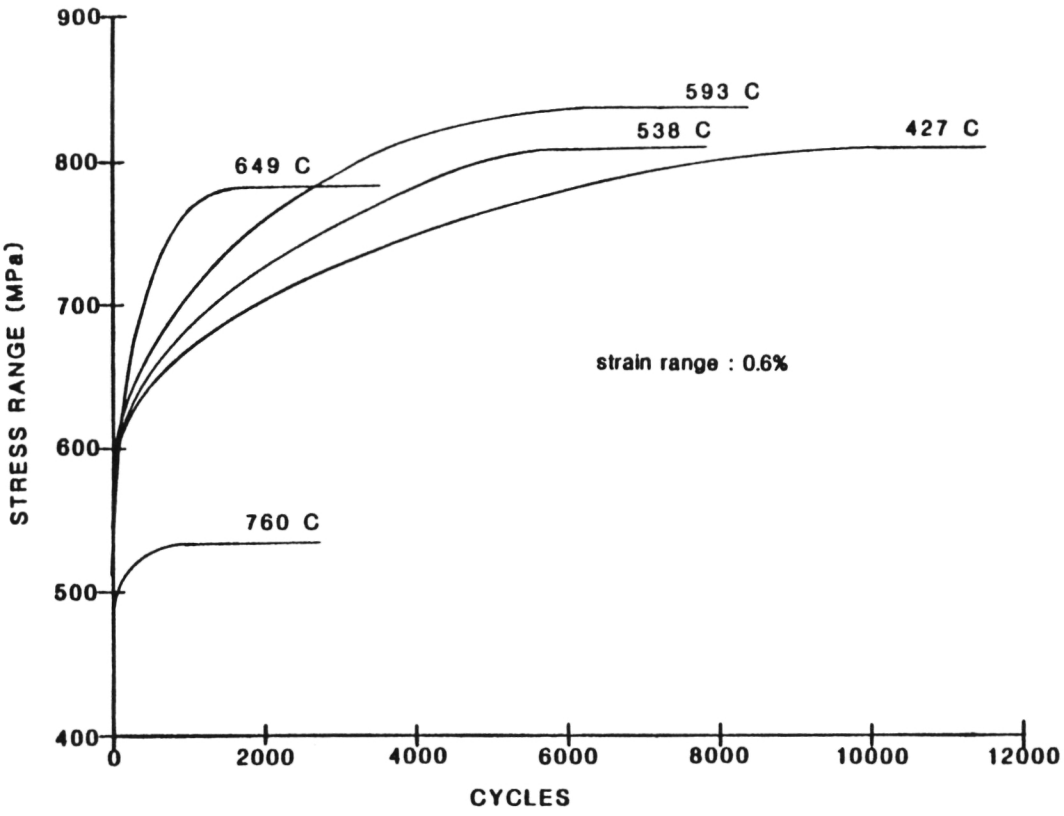

FIGURE 3.12 Results of Isothermal Cyclic Stress-Strain Tests

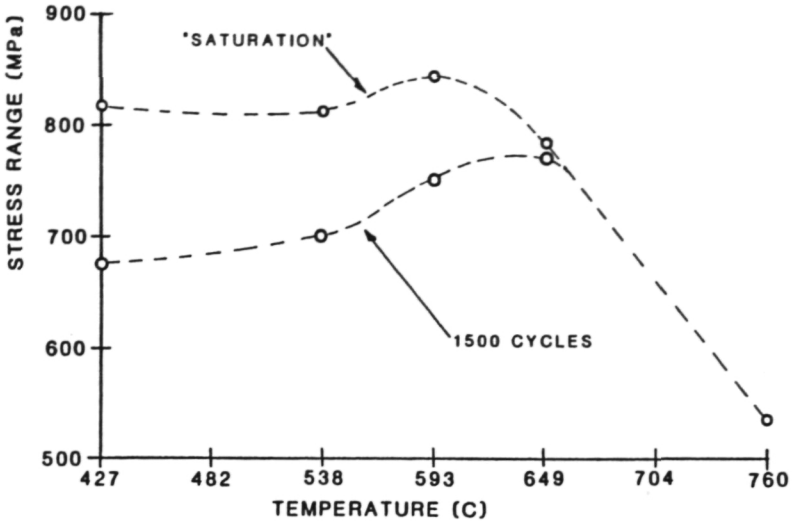

FIGURE 3.13 Results of Isothermal Cyclic Stress-Strain Tests Showing "Strain Aging Peak .

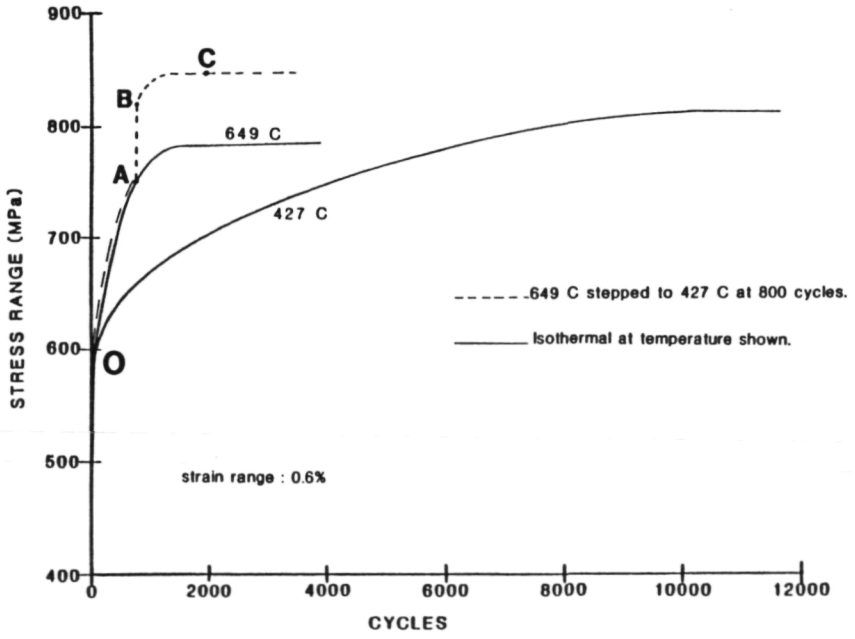

FIGURE 3.14 Results of Isothermal and Stepwise Cyclic Stress-Strain Tests Conducted at 427 and 649 C

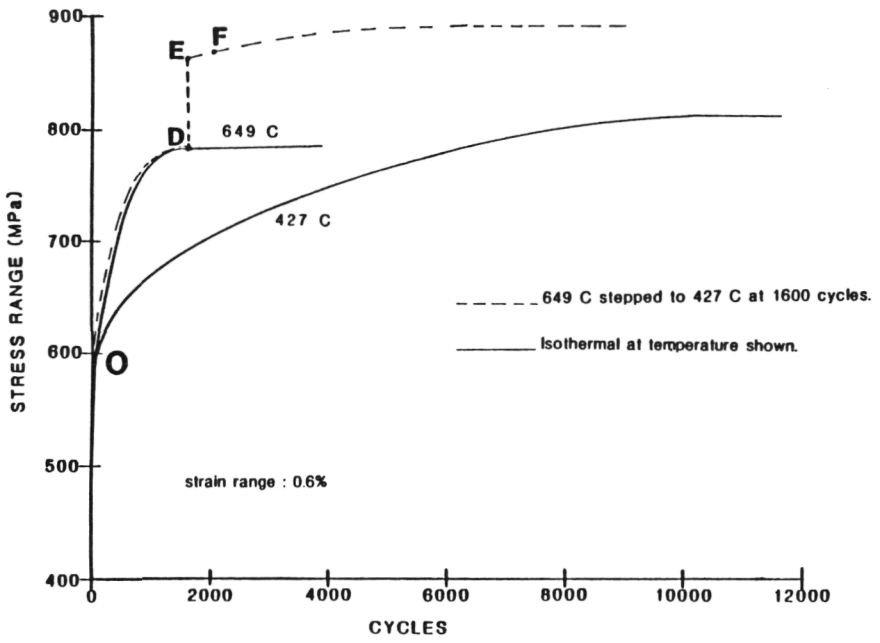

FIGURE 3.15 Results of Isothermal and Stepwise Cyclic Stress-Strain Tests Conducted at 427 and 649 C

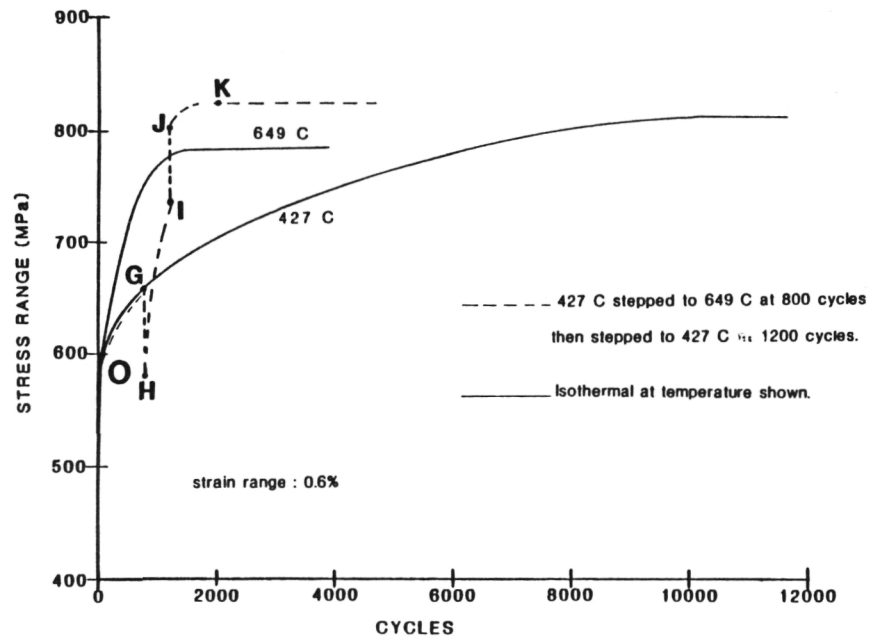

FIGURE 3.16 Results of Isothermal and Stepwise Cyclic Stress-Strain Tests Conducted at 427 and 649 C

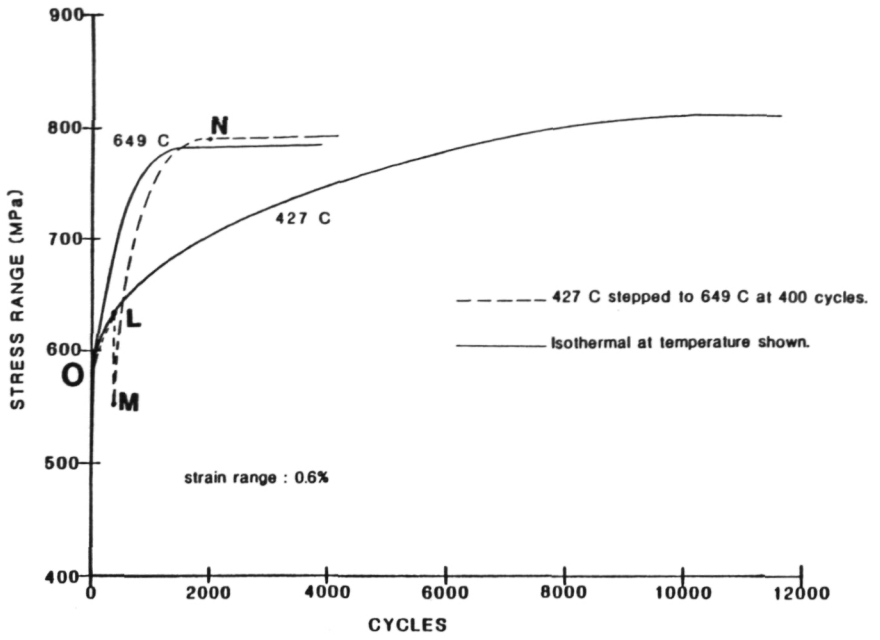

FIGURE 3.17 Results of Isothermal and Stepwise Cyclic Stress-Strain Tests Conducted at 427 and 649 C

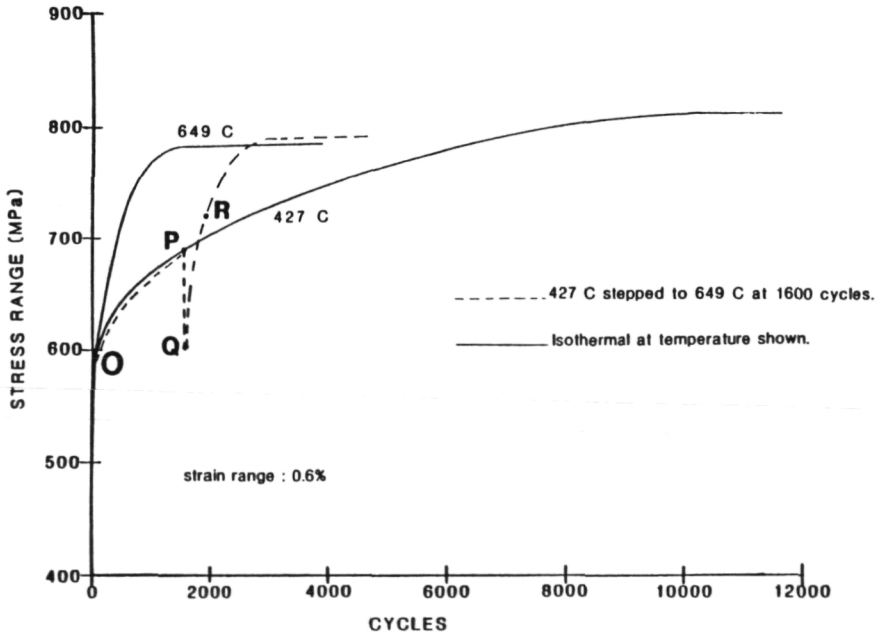

FIGURE 3.18 Results of Isothermal and Stepwise Cyclic Stress-Strain Tests Conducted at 427 and 649 C

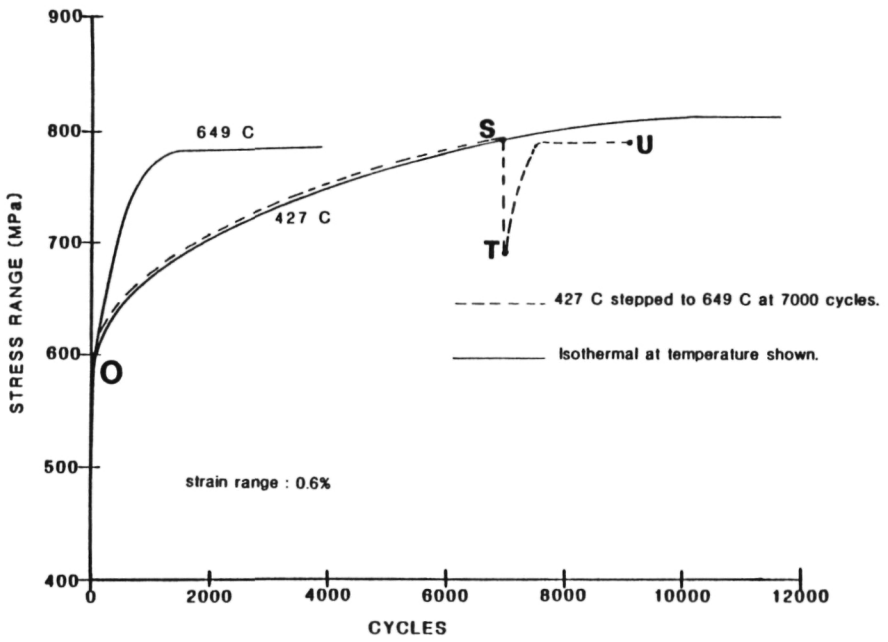

FIGURE 3.19 Results of Isothermal and Stepwise Cyclic Stress-Strain Tests Conducted at 427 and 649 C

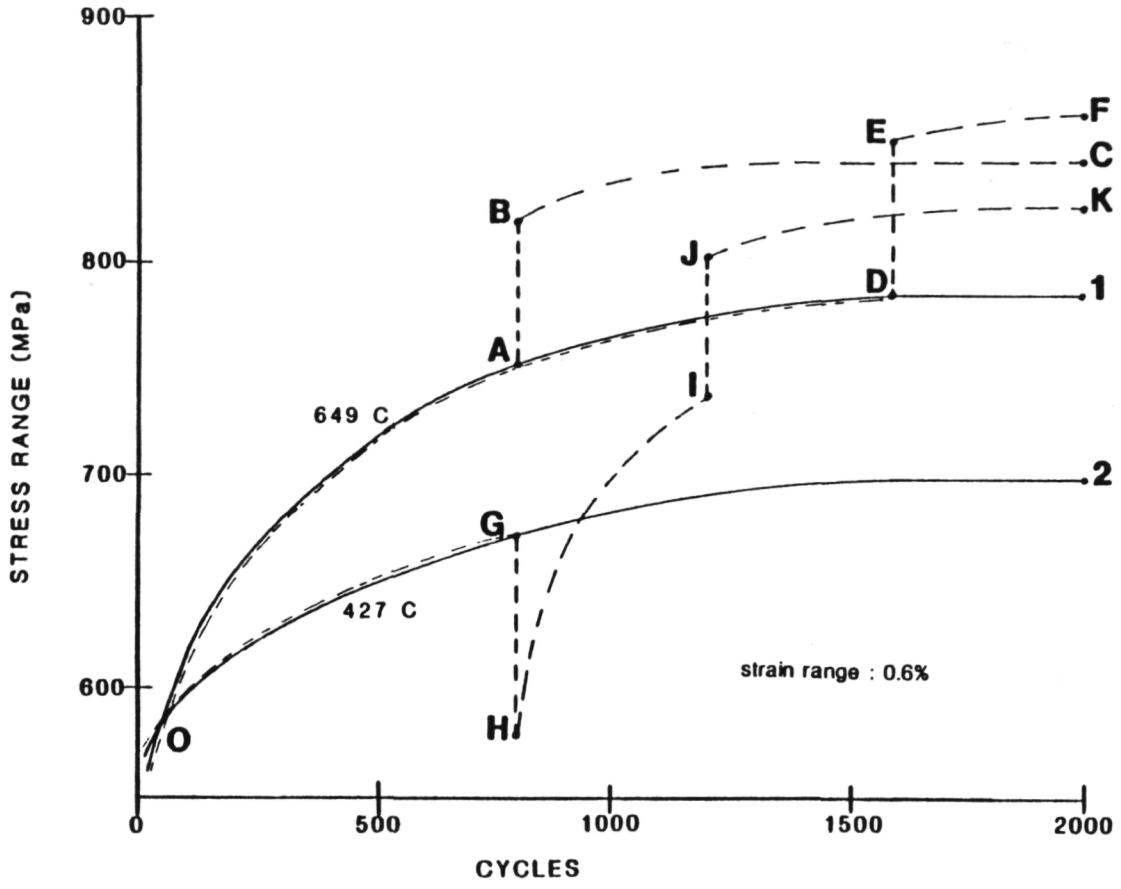

FIGURE 3.20 Results of the First 2000 Cycles of Figures 3.14 thru 3.16.

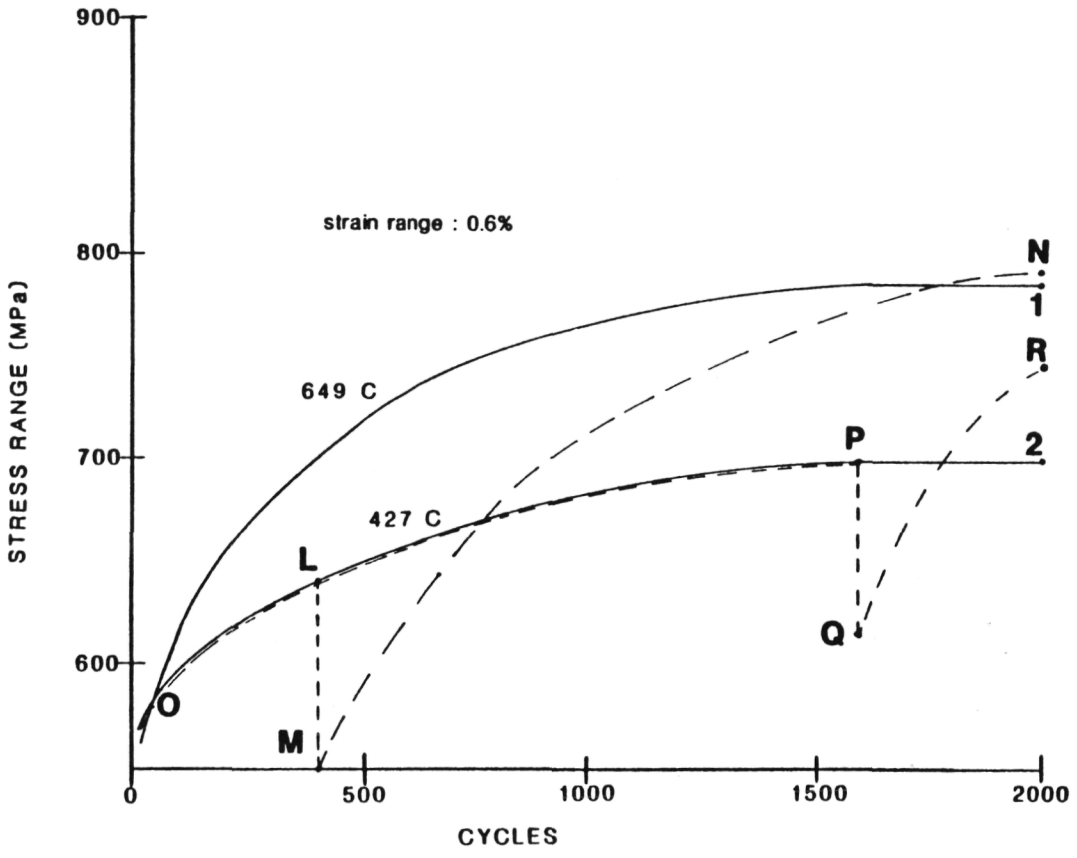

FIGURE 3.21 Results of the First 2000 Cycles of Figures 3.17 and 3.18.

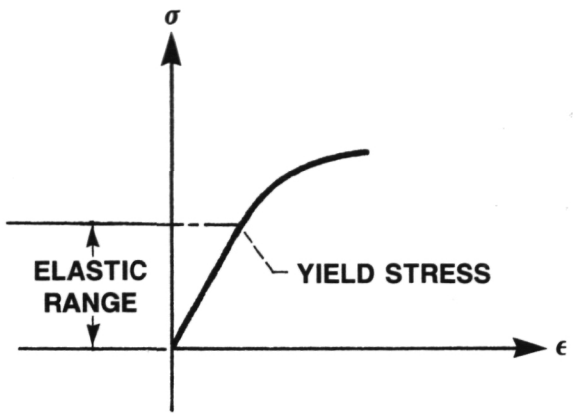

FIGURE A.1 Yield Point Representation.

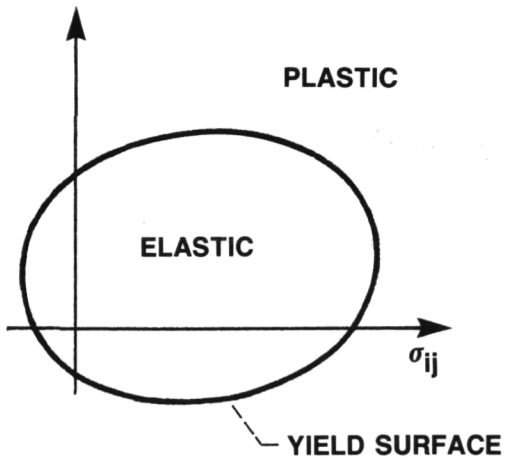

FIGURE A.2 Yield Surface Representation.

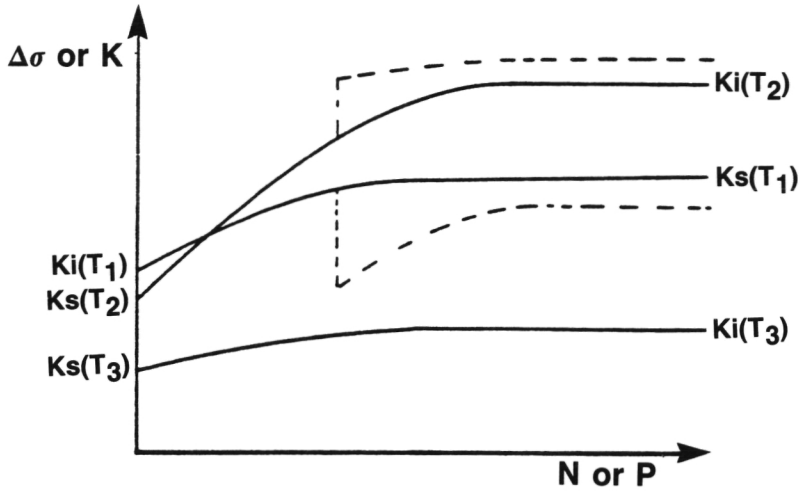

FIGURE 4.1 Typical Isothermal and Nonisothermal Hardening Curves.

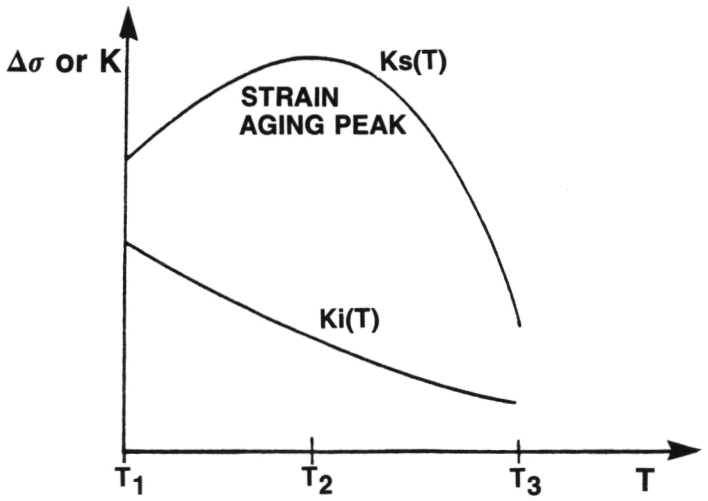

FIGURE 4.2 Typical Hardening vs Temperature Curve.

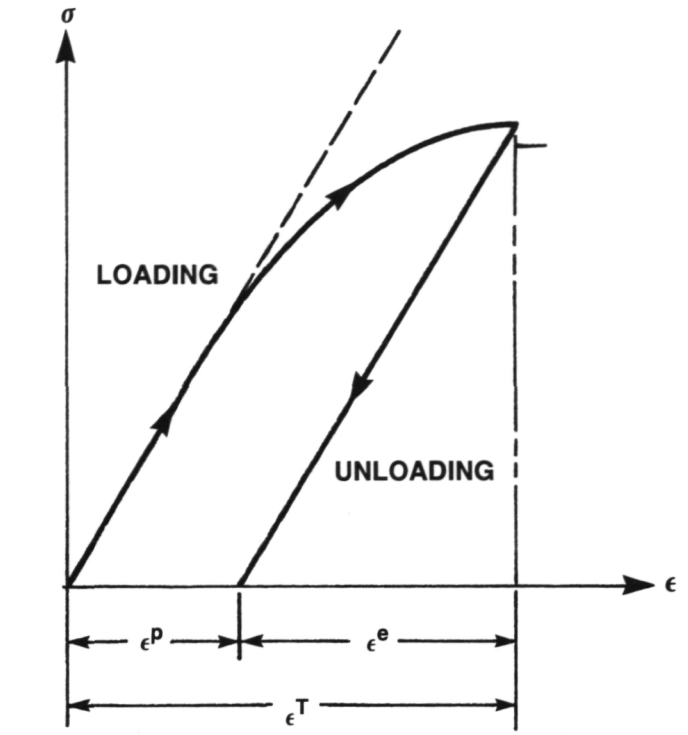

FIGURE A.3 Total Strain Partitioning.

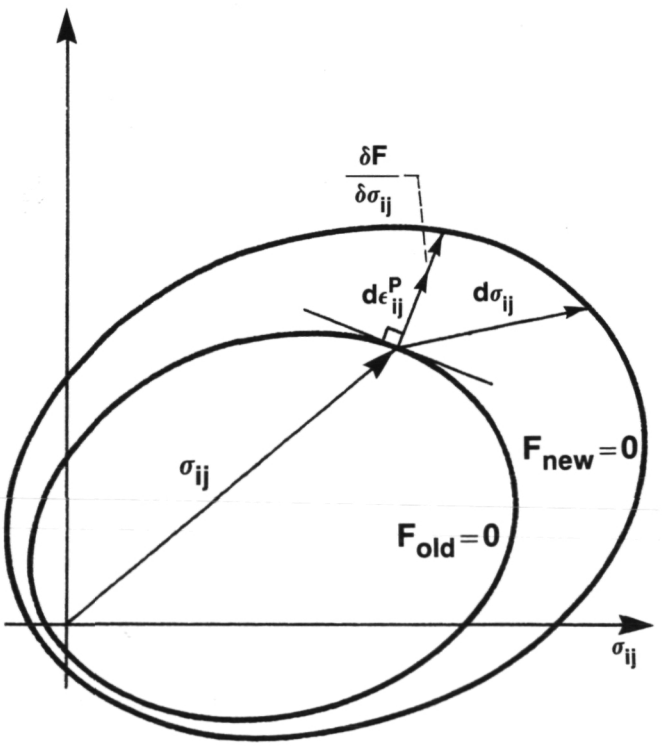

FIGURE A.4 Change in Yield Surface.

1. Report No.	2. Government Accession No.	3. Recipient's Catalog No.
NASA CR-174999		

4. Title and Subtitle	5. Report Date
Thermomechanical Cyclic Hardening Behavior of Hastelloy-X	November 1985
	6. Performing Organization Code
7. Author(s)	8. Performing Organization Report No.
Paul A. Bartolotta	
	10. Work Unit No.
9. Performing Organization Name and Address	11. Contract or Grant No.
The University of Akron Department of Civil Engineering Akron, Ohio	NAG 3-379
	13. Type of Report and Period Covered
12. Sponsoring Agency Name and Address	Contractor Report
National Aeronautics and Space Administration Washington, D.C. 20546	14. Sponsoring Agency Code
	505-33-7A

15. Supplementary Notes

Final report. Project Manager, Daniel J. Gauntner, Structures Division, NASA Lewis Research Center, Cleveland, Ohio. This report was submitted as a thesis in partial fulfillment of the requirements for the degree of Master of Science in Civil Engineering to the University of Akron, Akron, Ohio, in May 1985.

16. Abstract

Experimental evidence of thermomechanical history dependence on the cyclic hardening behavior of a representative combustor liner material Hastelloy-X is presented, along with a discussion about the relevant concept of thermomechanical path dependence. Based on the experimental results, a discussion is given on the inadequacy of formulating "nonisothermal" constitutive equations solely on the basis of isothermal testing. Finally, the essence of a mathematical representation of thermoviscoplasticity is presented that qualitatively accounts for the observed hereditary behavior. This is achieved by formulating the scaler evolutionary equation in an established viscoplastic theory to reflect thermomechanical path dependence. Although the necessary nonisothermal tests for further quantifying the thermoviscoplastic model have been identified, such data are not yet available.

17. Key Words (Suggested by Author(s))	18. Distribution Statement
Thermomechanical path dependence; Viscoplasticity; Thermoviscoplasticity; Constitutive theory; Stepwise nonisothermal	Unclassified - unlimited STAR Category 39

19. Security Classif. (of this report)	20. Security Classif. (of this page)	21. No. of pages	22. Price*
Unclassified	Unclassified		

*For sale by the National Technical Information Service, Springfield, Virginia 22161

National Aeronautics and
Space Administration

Lewis Research Center
Cleveland, Ohio 44135

SECOND CLASS MAIL

ADDRESS CORRECTION REQUESTED

Official Business
Penalty for Private Use $300

Postage and Fees Paid
National Aeronautics and
Space Administration
NASA-451

NASA